

¹ **GLO-Roots: an imaging platform enabling multidimensional characterization of soil-grown roots systems**

³ Rubén Rellán-Álvarez^{1, 9}, Guillaume Lobet², Heike Lindner^{1, 8}, Pierre-Luc Pradier^{1, 8, 10},
⁴ Jose Sebastian^{1, 8}, Muh-Ching Yee¹, Yu Geng^{1, 7}, Charlotte Trontin¹, Therese LaRue³,
⁵ Amanda Schrager-Lavelle⁴, Cara H. Haney⁵, Rita Nieu⁶, Julin Maloof⁴, John P. Vogel⁷,
⁶ José R. Dinneny^{1, 12}

⁷ ¹ Department of Plant Biology, Carnegie Institution for Science, Stanford, CA, USA.

⁸ ² PhytoSystems, University of Liège, Liège, Belgium.

⁹ ³ Department of Biology, Stanford University, Stanford, CA, USA.

¹⁰ ⁴ Department of Plant Biology, UC Davis, Davis, CA, USA.

¹¹ ⁵ Harvard Medical School, Massachusetts General Hospital, Department of Genetics, De-
¹² partment of Molecular Biology Boston, MA, USA

¹³ ⁶ USDA Western Regional Research Center, Albany, CA, USA

¹⁴ ⁷ DOE Joint Genome Institute, Walnut Creek, CA, USA

¹⁵ ⁸ These authors contributed equally

¹⁶ ⁹ Present address: Laboratorio Nacional de Genómica para la Biodiversidad (Langebio),
¹⁷ Unidad de Genómica Avanzada, Centro de Investigación y de Estudios Avanzados del Insti-
¹⁸ tuto Politécnico Nacional (CINVESTAV-IPN), Irapuato, Guanajuato, México

¹⁹ ¹⁰ Present address: Boyce Thompson Institute for Plant Research/USDA, Ithaca, NY, USA.

²⁰ ¹¹ Present address: Energy Biosciences Institute, UC, Berkeley, CA, USA

²¹ ¹² Corresponding author

²² **Author contributions:**

²³ RR-A: Conception, design and development of the growth and imaging system and Arabidop-
²⁴ sis transgenic lines; acquisition, analysis and interpretation of data; drafting and revising

25 the article.

26 GL: Development of the GLO-RIA image analysis plugin, analysis and interpretation of

27 data, drafting and revising the article.

28 HL: Acquisition of data, development of the tomato growth and imaging setup.

29 P-LP: Acquisition of data, analysis and interpretation of data

30 JS: Development of Brachypodium transgenic lines, acquisition and analysis of Brachy-

31 podium, Arabidopsis and tomato data.

32 MCY: Development of Arabidopsis and Brachypodium transgenic lines.

33 YG: Development of Arabidopsis transgenic lines.

34 CT: Acquisition and analysis of the QPCR data

35 TL: Acquisition and analysis of the QPCR data

36 AS-L: Contributed the unpublished dual-color tomato line.

37 CH: Contributed the unpublished *Pseudomonas fluorescens* CH267-lux strain.

38 RN: Contribution to the development of the Brachypodium transgenic line.

39 JM: Contributed the unpublished dual-color tomato line.

40 JPV: Contribution to the development of the Brachypodium transgenic line.

41 JRD: Conception, design and development of the growth and imaging system and Arabidop-

42 sis transgenic lines; acquisition, analysis and interpretation of data; drafting and revising

43 the article.

44 All authors read and approve the final version of the manuscript.

45 **Abstract**

46 Root systems develop different root types that individually sense cues from their local

47 environment and integrate this information with systemic signals. This complex multi-

48 dimensional amalgam of inputs enables continuous adjustment of root growth rates, direc-
49 tion and metabolic activity that define a dynamic physical network. Current methods for
50 analyzing root biology balance physiological relevance with imaging capability. To bridge
51 this divide, we developed an integrated imaging system called Growth and Luminescence
52 Observatory for Roots (GLO-Roots) that uses luminescence-based reporters to enable stud-
53 ies of root architecture and gene expression patterns in soil-grown, light-shielded roots. We
54 have developed image analysis algorithms that allow the spatial integration of soil prop-
55 erties such as soil moisture with root traits. We propose GLO-Roots as a system that
56 has great utility in presenting environmental stimuli to roots in ways that evoke natural
57 adaptive responses and in providing tools for studying the multi-dimensional nature of such
58 processes.

59 **Introduction**

60 Plant roots are three-dimensional assemblies of cells that coordinately monitor and acclimate
61 to soil environmental change by altering physiological and developmental processes through
62 cell-type and organ-specific regulatory mechanisms^{1,2}. Soil comprises a complex distribution
63 of particles of different size, composition and physical properties, airspaces, variation in
64 nutrient availability and microbial diversity^{3,4}. These physical, chemical and biological
65 properties of soil can vary on spatial scales of meters to microns, and on temporal scales
66 ranging from seasonal change to seconds. Root tips monitor this environment through
67 locally and systemically acting sensory mechanisms^{5,6}.

68 The architecture of the root system determines the volume of soil where resources can be
69 accessed by the plant (rhizosphere) and is under both environmental and genetic control.
70 Plasticity in growth parameters allows the plant to adjust its form to suit a particular soil.
71 Lateral roots, which usually make up the majority of the total root system, often grow at an
72 angle divergent from the gravity vector. This gravity set-point angle (GSA) is controlled by
73 auxin biosynthesis and signaling and can be regulated by developmental age and root type⁷.
74 Recent cloning of the *DRO1* Quantitative Trait Locus (QTL) demonstrates that natural

75 genetic variation is a powerful tool for uncovering such control mechanisms⁸.

76 Specific root ideotypes (idealized phenotypes) have been proposed to be optimal for acquisi-
77 tion of water and nitrogen, which are distinct from ideotypes for low phosphorus. Based on
78 computational modeling and field studies, the “steep, deep and cheap” ideotype proposed by
79 Lynch and colleagues may provide advantages to the plant for capturing water and elements
80 like nitrogen that are water soluble and therefore tend to move in the soil column with water.
81 This ideotype consists of highly gravitropic, vertically oriented roots that grow deep in the
82 soil column and develop large amounts of aerenchyma, which reduces the overall metabolic
83 cost of the root system³. Other nutrients, like phosphorus, which have limited water solu-
84 bility and are tightly bound to organic matter, usually accumulate in the top layers of soil
85 and favor root systems that are more highly branched and shallow. The low-phosphorus
86 ideotype effectively increases root exploration at the top layers of soil³. Modeling of root
87 system variables shows that optimum architecture for nitrogen and phosphorus uptake are
88 not the same⁹ and suggests tradeoffs that may affect the evolution of root architecture as a
89 population adapts to a particular environmental niche.

90 Clearly, understanding the architecture of root systems and how environmental conditions
91 alter root developmental programs is important for understanding adaptive mechanisms of
92 plants and for identifying the molecular-genetic basis for different response programs. In
93 addition, root systems have complexity beyond their architecture that needs to be incorpo-
94 rated into our understanding of plant-environment interactions. Primary and lateral roots
95 exhibit different stress response programs in *Arabidopsis*² and may play specialized roles
96 in water and nutrient uptake. Thus, it is important to develop methods that allow for a
97 multidimensional characterization of the root system that includes growth, signaling, and
98 interactions with other organisms. Furthermore, physiological parameters that affect whole
99 plant responses to the environment, such as transpiration, are likely integrated into such
100 processes, thus requiring a more holistic approach to studies of root function.

101 Based on these considerations we have developed a new root imaging platform, Growth
102 and Luminescence Observatory for Roots (GLO-Roots), which allows root architecture and

103 gene expression to be studied in soil-grown plants. GLO-Roots is an integrated system
104 composed of custom growth vessels, luminescent reporters and imaging systems. We use
105 rhizotrons that have soil volumes equivalent to small pots and support growth of Arabidopsis
106 from germination to senescence. To visualize roots, we designed plant-codon optimized
107 luciferase reporters that emit light of different wavelengths. To visualize reporter expression,
108 plants are watered with a dilute luciferin solution and imaged afterwards. We have built
109 a custom luminescence imaging system that automatically captures images of rhizotrons
110 held vertically. The signal from each reporter is distinguished using band-pass filters held
111 in a motorized filter wheel, which enables automated acquisition of images from plants
112 expressing both structural and environmentally and developmentally responsive reporters.
113 We have also developed GLO-RIA (GLO-Roots Image Analysis), an ImageJ¹⁰ plugin that
114 allows for automated determination of root system area, convex hull, depth, width and
115 directionality, which quantifies the angle of root segments with respect to gravity. GLO-
116 RIA is also able to relate root system parameters to local root-associated variables such as
117 reporter expression intensity and soil-moisture content.

118 Overall GLO-Roots has great utility in presenting environmental stimuli to roots in phys-
119 iologically relevant ways and provides tools for characterizing responses to such stimuli at
120 the molecular level in whole adult root systems over broad time scales.

121 **Box 1.**

122 All resources for GLO-Roots, including the original raw data used in the manuscript, sample
123 images, GLO-RIA user manual, the latest software updates and the source code, can be
124 found at: <https://dinnenylab.wordpress.com/glo-roots/>

125 **Results**

126 We have developed an integrated platform for growing, imaging and analyzing root growth
127 that provides advances in physiological relevance and retains the ability to visualize aspects

¹²⁸ of root biology beyond structure.

¹²⁹ **The GLO-Roots platform**

¹³⁰ GLO-Roots is comprised of four parts: i) growth vessels called rhizotrons that allow plant
¹³¹ growth in soil and root imaging; ii) luminescent reporters that allow various aspects of root
¹³² biology to be tracked in living plants; iii) GLO1 luminescence-imaging system designed to
¹³³ automatically image rhizotrons; iv) GLO-RIA, an image analysis suite designed to quantify
¹³⁴ root systems imaged using GLO-Roots.

¹³⁵ **Plant growth system** GLO-Roots utilizes custom designed growth vessels classically
¹³⁶ known as rhizotrons, which hold a thin volume of soil between two sheets of polycarbon-
¹³⁷ ate plastic. Acrylic spacers provide a 2-mm space in which standard peat-based potting
¹³⁸ mix is added. Black vinyl sheets protect roots from light and rubber U-channels clamp
¹³⁹ the rhizotron materials together. Plastic racks hold the rhizotrons vertically and further
¹⁴⁰ protect the roots from light. Rhizotrons and rack are placed in a black tub and water are
¹⁴¹ added, to a depth of about 2 cm, at the bottom to maintain moisture in the rhizotrons
¹⁴² during plant growth. The volume of soil in the rhizotrons (100 cm^3) is similar to small pots
¹⁴³ commonly used for *Arabidopsis* and supports growth throughout the entire life cycle (Fig
¹⁴⁴ 1A-C and Supplement 1). To determine how the biology of plants grown in rhizotrons com-
¹⁴⁵ pares to other standard growth systems, we utilized high-throughput qRT-PCR to study
¹⁴⁶ how these conditions affect expression of 77 marker genes in root and shoot samples. These
¹⁴⁷ genes were curated from the literature and belong to a wide array of biological pathways
¹⁴⁸ including nutrient acquisition, hormone and light response and abiotic stress. Whole roots
¹⁴⁹ and shoot samples were collected at the end of the light and dark periods (Long-day condi-
¹⁵⁰ tions: 16 hour light, 8 hours dark) from plants grown in rhizotrons, pots, and petri dishes
¹⁵¹ with two different media compositions (1X Murashige and Skoog basal salts (MS), 1% su-
¹⁵² crose or 0.25X MS, no sucrose). Principal component analysis of the gene expression values
¹⁵³ showed a separation of soil and gel-grown root systems in the the first principal compo-
¹⁵⁴ nents (Figure 1-figure supplement 1A). In roots grown on gel-based media, we observed

enhanced expression of genes associated with light-regulated pathways (flavonoid biosynthesis: *FLAVINOL SYNTHASE1*, *FLS1*, *CHALCONE SYNTHASE*, *CHS* and photosynthesis: *RUBISCO SUBUNITS1A*, *RBCS1A*, *CYCLOPHILIN 38*, *CYP38*), which is expected due to the exposure of gel-grown roots to light. In addition, genes associated with phosphorus nutrition (*LOW PHOSPHATE RESPONSE1*, *LPR1*, *PHOSPHATE STARVATION RESPONSE1*, *PHR1*) were (Figure 1-figure table supplement 1) less expressed in soil-grown roots, suggesting differences in nutrient availability between the different growth systems. Interestingly, shoot samples were not clearly distinguished by growth media and, instead, time of day had a greater effect (Figure 1-Supplement 2). These data suggest root systems may be particularly sensitive to media conditions and indicate that rhizotron-grown root systems more closely approximate the biology of pot-grown plants than standard gel-based media. Shoot weight and primary root length were significantly reduced for gel-grown plants compared to rhizotron- or pot-grown plants suggesting significant differences in the biology of plants grown under these conditions (Figure 1-figure supplement 1B-C). While the 2 mm depth of the soil sheet is 10 to 20 times the average diameter of an Arabidopsis root (between 100-200 microns¹¹), we evaluated whether rhizotron-grown plants exhibited any obvious stress as a consequence of physical constriction. We compared traits of plants growing in vessels that hold similar volumes of soil but in different volumetric shapes. The number of lateral roots was significantly lower in pot and cylinder-grown plants compared to rhizotron-grown plants (Figure 1-figure supplement 1D) whereas primary root length of rhizotron and cylinder-grown plants was significantly greater than pot-grown plants (Figure 1-figure supplement 1E). No significant differences in shoot area were observed between the three systems (Figure 1-figure supplement 1-data). Thus, these data do not support the hypothesis that rhizotron-grown plants experience physical constriction greater than other vessels holding the same volume of soil.

Generation of transgenic plants expressing different luciferases Arabidopsis roots cannot easily be distinguished from soil using brightfield imaging due to their thinness and translucency (Figure 1-figure supplement 3); thus, reporter genes are needed to enhance the

183 contrast between the root and their environment. Luciferase is an ideal reporter to visualize
184 roots: 1) unlike fluorescent reporters, luciferase does not require high-intensity excitation
185 light, which could influence root growth, 2) peat-based soil (a type of histosol) exhibits no
186 autoluminescence but does autofluoresce at certain excitation wavelengths similar to GFP
187 (Figure 1-figure supplement 3), 3) while GFP is very stable, and thus not as suitable for
188 imaging dynamic transcriptional events, the luciferase enzyme is inactivated after catabolism
189 of luciferin, making it ideal for studying processes such as environmental responses. A
190 considerable number of luciferases have been developed that emit light spanning different
191 regions of the visible spectrum, but their utilization has been limited to studies in animals
192 (Table 1).

193 To determine the efficacy of using luciferase to visualize roots in soil, we codon optimized
194 sequences of *PpyRE8*, *CBGRed*, *LUC2*, and *CBG99* for Arabidopsis expression. In addition,
195 nanoLUC and venus-LUC¹² were utilized. Constitutive luciferase expression was driven
196 in plants using the *UBIQUITIN 10* (*UBQ10*) or *ACTIN2* (*ACT2*) promoters using vectors
197 assembled through a Golden-Gate cloning system¹³. Plants homozygous for a single locus
198 T-DNA insertion were evaluated for in vivo emission spectra and luminescence intensity
199 (Fig 1D). All the evaluated luciferases use D-luciferin as a substrate facilitating the simulta-
200 neous imaging of different luciferases except nanoLUC, which uses a proprietary substrate
201 furimazine¹⁴. In general, luciferases with red-shifted emission spectra were less intense than
202 the green-shifted luciferases (Fig 1D). LUC2o showed an emission maximum at 580 nm and
203 a minor peak at 620 nm while CBG99o lacks the minor peak.

204 Continuous addition of luciferin did not have any significant effect on shoot weight or primary
205 root length (Figure 1-figure supplement 4). After luciferin addition, luminescence signal
206 could be reliably detected in root systems for up to 10 days, depending on the developmental
207 state of the plant.

208 **GLO1: a semi-automated luminescence imaging system for rhizotrons** Lumines-
209 cence imaging systems commercially available for biomedical research are usually optimized

for imaging horizontally held specimens or samples in microtiter plates. Placing rhizotrons in this position would induce a gravitropic response in plants. Working with Bioimaging Solutions (San Diego, CA) we designed and built a luminescence imaging system optimized for rhizotron-grown plants. GLO1 (Growth and Luminescence Observatory 1) uses two back-thinned CCD cameras (Princeton Instruments, USA) to capture partially-overlapping images of rhizotrons while a motorized stage automatically rotates the rhizotron to capture images of both sides (Fig 1E). A composite image is generated from the images captured of each side; Fig 1F shows that approximately half of the root system is revealed on each side with few roots being visible on both sides. Apparently, the soil sheet is thick enough to block portions of the root system but thin enough to ensure its continuous structure can be compiled from opposite face views. We tested the ability of GLO1-generated images to reveal complete root systems by manually quantifying the number of lateral roots in excavated root systems of 8 different plants and testing these results against estimates of lateral root number from images of the same plants visually inspected by 4 different persons. These comparisons revealed good correlation ($(R^2 = 0.974)$) between actual lateral root counts and image-based estimation, indicating GLO1-generated root images provide an accurate representation of the in soil root system.

GLO-RIA: GLO-Roots Image Analysis We developed a set of image analysis algorithms that were well suited for the complex root systems that GLO-Roots is able to capture. GLO-RIA (Growth and Luminescence Observatory Root Image Analysis) is an ImageJ plugin divided in two modules. The first module (RootSystem) performs four different types of analysis: i) a local analysis that detects all root particles in the image and computes their position, length and direction; ii) the global analysis performs a root system level analysis and computes the total visible surface, convex hull, width and depth; iii) the shape analysis uses Elliptic Fourier Descriptors or pseudo-landmarks similarly to RootScape¹⁵ to perform a shape analysis on the root system iv) the directionality analysis computes the mean direction of root particles in a root system (either on the full image or by a user-defined region of interest in the image). These four analysis methods are fully automated by default, but

238 can be manually adjusted if needed. The second module of GLO-RIA (RootReporter) was
239 specifically designed for the analysis of multi-layered images such as combinations of gene
240 reporter, root structure and soil moisture. Shortly, the plugin works as follows: i) detection
241 of the gene reporters and the structure reporters in their respective images; ii) if needed, a
242 manual correction can be performed to correct the automated detection; iii) gene reporters
243 are linked with the soil water content and the structure reporters, based on their proximity;
244 iv) gene reporter intensity (either absolute or normalized using the structural reporter) is
245 computed; v) all data are exported and saved to a RSML datafile¹⁶. Gene and structure
246 reporters can be followed across different time and space points. Using an object oriented
247 approach, great care has been taken to facilitate the user interactions on the different images
248 to streamline the analysis process. Table 2 shows a list of root system features extracted
249 using GLO-RIA. GLO-RIA does not currently have the ability to reconstruct the root archi-
250 tecture in itself (topological links between roots). This is a challenge for analyzing images
251 captured by GLO-Roots since soil particles cause disruption of root segments.

252 We tested the accuracy of the measurements obtained from GLO-RIA using two different
253 ground-truthed data sets. Manual measurement of root system width, depth and average
254 lateral root angle was determined by hand using imageJ from an independent set of images
255 corresponding to roots of several Arabidopsis accessions growing in control conditions. We
256 also used ArchiSimple¹⁷ to generate 1240 images of root system models with contrasting sizes
257 and lateral root angles. Since these images are computationally generated, exact determi-
258 nation of root system parameters was possible. For both ground truth data sets, GLO-RIA
259 quantification provided measurements that were well correlated for all all three measured
260 parameters (Figure 1-figure supplement 5D-F). Sample images of real and ArchiSimple gen-
261 erated root images shown with GLO-RIA-defined directionality color-coding (Figure 1-figure
262 supplement 5G-I).

263 Continuous imaging of root growth

264 The size of our rhizotrons enables undisturbed root system development (before roots reach
265 the sides or the bottom of the rhizotron) for about 21-23 days for the Col-0 accession
266 growing under long day conditions (Figure 2); however root traits such as directionality
267 can be observed through later stages of plant development. See 35 DAS root system and
268 directionality in Figure 2A-B. An example of a time series spanning 11 to 21 days after
269 sowing (DAS) of Col-0 roots expressing *ProUBQ10:LUC2o* is shown in Fig 2A and [Video 1](#)
270 with a color-coded time projection shown in Fig 2C. Directionality analysis (Fig 2B) shows
271 a progressive change in root system angles from 0 ° (vertical) to 45 ° as lateral roots take
272 over as the predominant root type. Figure 2D shows the evolution over time of several root
273 traits that can be automatically captured by GLO-RIA (depth, width, area) and others that
274 were manually quantified (primary root growth rate or number of lateral roots per primary
275 root).

276 Root system architecture of different *Arabidopsis* accessions.

277 As a proof of concept to estimate the utility of our root imaging system to phenotype
278 adult root system traits, we transformed a small set of accessions (Bay-0, Col-0 and Sha)
279 with the *ProUBQ10:LUC2o* reporter and quantified RSA at 22 DAS (Fig 3A-C). GLO-RIA
280 analysis of these root systems identified several root traits that distinguish Col-0, Bay-0
281 and Sha. Directionality analysis revealed an abundance of steep-angle regions in the root
282 system of Bay while Sha showed an abundance of shallow-angled regions and Col-0 was
283 intermediate (Fig 3D). Bay-0 shows the deepest and narrowest root system leading to the
284 highest depth/width ratio while Sha has the widest root system (Fig 3E). Other root traits
285 such as root system area and the vertical center of mass also showed significant differences
286 (Figure 3-figure supplement 1B). Broad sense heritability values for depth (96.3), area (92.0),
287 depth/width (97.8), width (95.7) and vertical center of mass (95.0) were all higher than 90%.
288 To capture the richness of root architecture shape, we used GLO-RIA to extract pseudo-
289 landmarks describing the shape of the root system (see Materials and Methods for more

290 details) and performed PCA analysis. The first principal component captures differences
291 in the distribution of widths along the vertical axis and separates Col-0 and Sha from Bay-
292 0 root systems. (Fig 3F). Bay-0 shows an homogenous distribution of widths along the
293 vertical axis while Sha and Col-0 are much wider at the top than bottom. PC2 seems to be
294 capturing a relationship between width at the top and total depth and separates Sha root
295 systems which are wide at the top and deep from Col-0 root systems which are wide but
296 not as deep as Sha. Shape information extracted from pseudo-landmarks can distinguish
297 the three different accession using PCA analysis (Fig 3G)

298 **Spectrally distinct luciferases enable gene expression patterns, characterization**
299 **of root system interactions and microbial colonization.**

300 We tested whether spectrally distinct luciferase reporters would enable additional informa-
301 tion besides root architecture to be captured from root systems. Luciferase reporters have
302 been commonly used to study gene expression and these resources can potentially be utilized
303 to study such regulatory events in soil-grown roots. We transformed *ProACT2:PpyRE8o*
304 into two well studied LUC reporter lines: the auxin response reporter line *ProDR5:LUC*¹⁸
305 (Figure A-B) and the Reactive Oxygen Species (ROS) response reporter *ProZAT12:LUC*¹⁹
306 (Figure 4C-D). We implemented in GLO-RIA an algorithm that semi-automatically iden-
307 tifies gene reporter signal and associates this object to the corresponding root structure
308 segment. A graphical representation of the results obtained with Root Reporter can be
309 observed in Figure 4-figure supplement 1. Reporter intensity values along the first 5 mm
310 of root tips can also be observed in Figure 4-figure supplement 2. We then took advantage
311 of our ability to constitutively express two spectrally different luciferases and imaged the
312 overlapping root systems (one expressing *ProUBQ10:LUC2o* and the other *ProACT2:PPy*
313 *RE8o*). While two root systems were distinguishable using this system (Figure 4-figure sup-
314 plement 3); measurements of root system area did not reveal a significant effect on root
315 growth when two plants were grown in the same rhizotron, compared to one; however, fur-
316 ther studies are warranted (Figure 4-figure supplement 3).

317 The GLO-Roots system uses non-sterile growth conditions, which allows complex biotic
318 interactions that may affect responses to the environment. Bacteria themselves can be en-
319 gineered to express luminescent reporters through integration of the LUX operon, which
320 results in luminescence in the blue region of the spectrum and is thus compatible with
321 the plant-expressed luciferase isoforms we have tested. *Pseudomonas fluorescens* CH267²⁰,
322 a natural *Arabidopsis* root commensal, was transformed with the bacterial LUX operon
323 and used to inoculate plants. Thirteen days after inoculation, we were able to observe
324 bacterial luminescence colocalizing with plant roots. *P. fluorescens* did not show an ob-
325 vious pattern of colonization at the root system scale level. As a proof-of-principle test
326 of the multi-dimensional capabilities of the GLO-Roots system we visualized both *LUC2o*
327 and *PPyRE8o* reporters in plants and the LUX reporter in bacteria in the same rhizotron
328 (Figure 4-figure supplement 4).

329 **Adaptive changes in root system architecture under water deprivation, phos-
330 phorus deficiency and light** To test the utility of the GLO-Roots system to understand
331 response of root systems to environmental stimuli we tested the effects of light and condi-
332 tions that mimic drought and nutritional deficiency. To examine the effects of light exposure
333 on the root architecture, the black shields, which normally protect the soil and roots from
334 light, were removed from the top half of the rhizotrons 10 DAS. Using directionality analysis
335 we detected a significant increase in the steepness of roots only in the light exposed region of
336 the rhizotron, while the lower shielded region showed no difference. (Fig 6-figure supplement
337 3A-B and Fig 6-figure supplement 4). Light can penetrate the top layers of soil²¹ and it
338 has been proposed to have a role in directing root growth specially in dry soils²² through
339 the blue light receptor *phot1*. Root directionality was not significantly different between
340 light and dark-treated roots of the *phot1/2* double mutant suggesting that blue light per-
341 ception is necessary for this response^{22,23} (Fig 6-figure supplement 3B-lower panel). These
342 data highlight the strong effects of light on root system architecture²⁴, which GLO-Roots
343 rhizotrons are able to mitigate.

344 Plants grown in low-P soil showed a significant increase in the width-depth ratio of the root

345 system compared to plants grown in P-replete soil, as determined using the automated root
346 system area finder in GLO-RIA (Fig 6-figure supplement 2A-B). Plants under P deficiency
347 showed an increase in the ratio between root-shoot area (Fig 6-figure supplement 2C) and
348 higher investment of resources in the development of the root system at the expense of shoot
349 growth (Fig 6-figure supplement 2D). Root systems of control and P-deficient plants showed
350 no significant differences in directionality at 22 DAS but at 27 DAS, roots were more hori-
351 zontally oriented in P-deficient plants (Fig 6-figure supplement 2E). The observed changes in
352 root architecture are consistent with root system ideotypes that improve phosphorus uptake
353 efficiency.

354 GLO-Roots is especially well suited for studying water-deficit (WD) responses. First, shoots
355 are exposed to the atmosphere and vapor pressure deficit (VPD) is maintained at levels that
356 allow for transpiration of water from the shoot. Second, soil in rhizotrons is exposed to air
357 at the top and dries basipetally (from the top-down); drying soil increases the volume
358 occupied by air and reduces contact of root with liquid water, all of which are similar to
359 changes in soil expected in the field during WD. Finally, as peat-based soil dries, its optical
360 properties change, allowing moisture content to be approximated from bright-field images.
361 We took advantage of the change in gray-scale pixel intensity to construct a calibration
362 curve (Figure 5-figure supplement 1) that quantitatively relates gray-scale pixel intensity to
363 moisture content (Fig 5A); water content can be color coded in images with appropriate
364 look up tables (Fig 5B). Soil color was not affected by the presence or absence of roots
365 (Figure 5-figure supplement 2). Using this approach, water content in a rhizotron can be
366 mapped and visualized in 2D (Fig 5C-D). In the example shown, we can observe that a 22
367 DAS Bay-0 plant depleted soil-moisture content locally around the the root system (Figure
368 5E).

369 We performed several trials to simulate WD in our growth system. Plants were germinated,
370 grown under control conditions then transferred to 29°C and standing water removed from
371 the container holding the rhizotrons starting at 9 DAS or 13 DAS. Elevated temperature
372 combined with water deficit is a common stress that modern crops varieties are poorly

adapted to, thus highlighting the importance of examining this combined treatment^{25,26}.
Plants were maintained in this WD regime until 22 DAS when luciferin solution was added
and the plants imaged. At 13 DAS, lateral roots near the soil surface are already emerged
([Video 1](#), Figure 2A) and 9 days of subsequent WD treatment caused lateral roots to show an
increase in gravitropism leading to the development of a root system that were deeper and
more vertically oriented (Fig 6A). Roots of Bay-0 plants showed similar responses, though
the extent of change was less pronounced since Bay-0 roots are normally more vertically
oriented (Fig 6B). Plants transferred at 9 DAS and grown for 13 days under WD showed
less lateral root development in the top layer of soil (Fig 6E). At this time point, lateral roots
start to emerge ([Video 1](#)) and early drought may lead to growth quiescence or senescence.
Careful examination of roots in these regions showed evidence of small lateral root primordia
populating the primary root (Figure 6F). After 24 h of re-watering (Figure 6G) these lateral
root primordia reinitiated growth (Figure 6H).

Time-lapse imaging of the water deficit response showed that changes in root growth direction
occurred ahead of the dry soil front [Video 2](#). Using GLO-RIA we were able correlate
local water moisture contents with the orientation of root segments. With this approach we
observed that root segments in dryer areas of rhizotron grew at steeper root angles (Figure
7) than roots in WW regions, though lateral root angle in wetter regions was also affected.
These data suggest that both local and systemic signaling is likely involved in redirecting
lateral roots deeper during the simulated drought treatments tested here.

We also grew plants under WD at control temperatures or under WW conditions at elevated
temperature to test the effects of these individual stresses on root architecture. We observed
that both conditions were sufficient to induce a change in root directionality indicating that
the plant uses similar mechanisms to avoid heat and water-deficit associated stresses (Figure
6-figure supplement 1). We next asked which regulatory pathways controlled the observed
changes in lateral root directionality during simulated drought. Hydrotropism is a known
environmental response that directs root growth towards wet regions of soil. MIZ1 is an
essential regulator of hydrotropism; however *miz1* mutants had no significant effect on water

401 deficit-induced changes in root directionality, compared to wild type (Fig 6C), indicating
402 that this response was distinct from hydrotropism. Auxin is an important mediator of
403 gravitropism and auxin treatment causes lateral roots to grow more vertically⁷. Consistent
404 with this role for auxin, mutant plants with loss of function in the auxin receptor TIR1, did
405 not show changes in the root system directionality between WW and WD conditions (Fig
406 6D).

407 **GLO-Roots for Brachypodium and Tomato.**

408 To examine the general applicability of the GLO-Roots system for other species, we intro-
409 duced LUC2o-expressing reporters into the model grass *Brachypodium distachyon* and the
410 crop plant *Lycopersicon esculentum* (tomato). Brachypodium is well suited to the GLO-Root
411 system because, like Arabidopsis, its small size allows mature root systems to be studied in
412 relatively small soil volumes^{27,28}. *LUC2o* driven by the *ZmUb1* promoter was introduced into
413 Brachypodium using the pANIC vector²⁹. Brachypodium roots showed a distinct architec-
414 ture from Arabidopsis marked by prolific development of secondary and tertiary lateral roots
415 (Fig 8A). This is consistent with other studies that show that Brachypodium has a typical
416 grass root system²⁸. Comparison of root system development in rhizotrons with gel-based
417 media showed that root growth is higher in soil than in plates (Figure 8-figure supplement
418 1). Previous work has suggested that auxin levels in Brachypodium roots is sub-optimal for
419 growth³⁰. Pacheco-Villalobos and colleagues suggest that, in Brachypodium, and contrary
420 to what happens in Arabidopsis, ethylene represses *YUCCA* reducing the synthesis of auxin.
421 The reduced growth that we observe in plates and the high levels of ethylene that build up
422 in sealed plates³¹ would support this mechanism.

423 Tomato plants were transformed with *Pro35S:PPyRE8o* and *ProeDR5rev:LUC2* reporters.
424 The plants showed more rapid growth than Arabidopsis or Brachypodium and required
425 fertilizer to prevent obvious signs of stress (reduced growth, anthocyanin accumulation).
426 Root systems were imaged from 17 DAS plants. Roots showed presumptive lateral root
427 primordia marked by DR5-expression (Fig 8C-D). These results show that the GLO-Roots

428 method can be applied to study root systems of plants and will likely be useful for studying
429 root systems of other small to medium sized model plants and for early stages of larger crop
430 plants.

431 **Discussion**

432 **GLO-Roots enables a multi-dimensional understanding of root biology**

433 Recent studies of root systems has emphasized structural attributes as important contrib-
434 utors of root system function. Indeed, studies examining the role of genetic variants in
435 tolerating abiotic stress have demonstrated the importance of such characteristics⁸. Roots,
436 however, are highly diverse in the biology they perform and a multi-dimensional understand-
437 ing of root systems, which incorporates differences in signaling, metabolism and microbial
438 association as well as structure, may provide a clearer understanding of the degree to which
439 sub-functionalization of the root system plays a role in important processes such as acclima-
440 tion and efficient resource acquisition.

441 We have developed tools in GLO-Roots that allow for tracking multiple aspects of soil
442 physicochemical properties and root biology simultaneously. Using GLO-Roots, we are able
443 to map in 2D coordinates soil physical properties such soil moisture together with root ar-
444 chitecture traits such as directionality, growth rates and gene expression levels. All this
445 information is aggregated in layers for each x, y coordinate. Using GLO-RIA we integrate
446 this multilayer information, leveraging our ability to simultaneously and seamlessly inves-
447 tigate root responses to environmental stimuli such as soil moisture content. Luciferase
448 isoforms that emit light at different wavelengths allow for constitutive and regulated pro-
449 moters to be studied together. Introduction of luciferase reporters into microbes provides
450 an additional layer of information that provides a readout on the association between or-
451 ganisms and how this might be affected by environmental conditions. The flexibility of the
452 GLO-Roots system may enable additional dimensionality to our understanding of root biol-
453 ogy. Other physical properties such as CO₂ or pH mapping in rhizotrons have already been

454 enabled by using planar optodes³². It may be possible to engineer LUX-based reporters
455 in microbes that are responsive to extracellular metabolites, creating microbial biosensors,
456 and integration of such tools may enable root-exudation and nutrition to be analyzed in
457 soil. Split-Luciferase reporters have been engineered that allow bi-molecular interactions to
458 be studied. Finally, molecular sensors analogous to FRET sensors, termed BRET-sensors³³,
459 may allow metabolite tracking dynamically through the root system. With additional innova-
460 tion in the development of luciferase reporters, the GLO-Roots systems will likely expand
461 the repertoire of biological processes that can be studied over an expanded range of devel-
462 opmental time points and environmental conditions.

463 **Enhanced root growth and gravitropism may constitute an avoidance mechanism
464 used during water deficit stress**

465 It has been proposed that plants with steep root systems will be better able to tap into deep
466 water resources and thus perform better under water deprivation. For example in rice, the
467 IR64 paddy cultivar shows shallow root systems in upland fields whereas Kinandang Patong,
468 an upland cultivar, is deeper rooting⁸. Plants maintain a number of regulatory pathways that
469 mediate changes in physiology during WD. Enhanced growth of root systems has been well
470 characterized in field-grown plants; however this has not been recapitulated in studies of gel-
471 grown Arabidopsis plants. Thus, it has been unclear whether Arabidopsis simply responds
472 to WD differently. Our results here show that Arabidopsis does indeed maintain a classical
473 WD response that expands the root system and directs growth downward. Interestingly,
474 under our stress regime, we did not observe a significant decrease in the relative water
475 content of shoot tissues (Figure 6-figure supplement 5), suggesting that the changes in root
476 architecture were sufficient to provide access to deep water and prevent dehydration. Such
477 changes in root growth are likely regulated through systemic and local signaling that involve
478 auxin signaling but acts independently of known pathways that control moisture-directed
479 root growth.

480 **Perspectives and Conclusions**

481 Understanding plant biology requires a sophisticated understanding of how environmental
482 stimuli affect the form and function of plants as well as an understanding of how physiological
483 context informs such responses. Environmental conditions are at least as complex as the
484 plants they affect. Plant roots are exposed to a variety of environmental signals that change
485 in time and space at very different scales that are integrated at the whole plant system. It is
486 an important challenge in biology to develop methods of growing and studying plants that
487 present such stimuli in a manner that the plant is likely to encounter in nature. After all, the
488 plants we study have evolved to survive through mechanisms that have been selected, over
489 evolutionary time, in nature. It will be interesting for future studies to determine how other
490 environmental stimuli affect root growth using GLO-Roots and whether these responses
491 differ between accessions of Arabidopsis. Identification of the genetic loci responsible for
492 phenotypic variation in adult root phenotypes may identify the molecular basis for adaptive
493 variation that exists in this species and potentially identify loci that are useful for breeding
494 efforts needed for the next green revolution.

495 **Materials and methods**

496 **Growth system**

497 **Rhizotrons and growth system fabrication.** Rhizotrons are composed of two sheets of
498 1/8" abrasion resistant polycarbonate plastic (Makrolon AR (R)) cut to size using a water
499 jet (AquaJet LLC, Salem, OR), two acrylic spacers cut using a laser (Stanford Product
500 Realization Lab), two rubber U-channels cut to strips 30 cm long ([McMaster Carr part](#)
501 [# 8507K33](#)) and two sheets of black 0.030" thick polypropylene sheets ([McMaster Carr](#)
502 [part # 1451T21](#)) cut with a straight-edge razor blade. Rhizotron designs were drafted in
503 Adobe Illustrator (Adobe, San José, CA). The blueprints of all the parts are provided in
504 Supplement 1. The top edge of each polycarbonate sheet was painted with black 270 Stiletto
505 nail polish (Revlon, New York, NY).

506 **Boxes and holders.** Rhizotrons are held vertical during plant growth in a custom rack sys-
507 tem composed of two sheets of 1/4" black acrylic plastic cut with slots for eleven rhizotrons
508 using a laser, four 3/8" PVC rods ([McMaster Carr part # 98871a041](#)) secured with PVC
509 nuts ([McMaster Carr part # 94806a031](#)) to hold the acrylic sheets horizontal. The rack is
510 placed inside a 12" x 12" x 12" black polyethylene tank ([Plastic Mart part # R121212A](#)).

511 **Rhizotron preparation** The procedure to construct a rhizotron with soil is as follows:
512 Two pieces of polycarbonate plastic are laid flat on a table with the spacers inserted. Using
513 an electric paint gun, a fine mist of water is applied to the bare polycarbonate sheets. Then,
514 using a 2 mm sieve (US Standard Sieve Series N° 10) a fine layer of PRO-MIX(r) PGX soil
515 (Premier Tech, Canada) is applied. Excess soil is discarded by gently tapping the plastic
516 against the table in a vertical position. Water is sprayed again onto the soil, then a second
517 layer of Pro-MIX is applied as before. For P deficiency experiments soil supplemented with
518 1 ml of 100 µM P-Alumina (control) and 0-P-Alumina (P deficient) was used. To prevent
519 the soil from falling out of the bottom opening, a 3 x 6 cm piece of nylon mesh is rolled into
520 a 1 cm wide tube and placed at the bottom side of the rhizotron. The spacers are removed
521 and replaced by clean spacers. The two faces of the rhizotron are carefully joined together
522 and two rubber U-channels slipped on to clamp all pieces together. Assembled rhizotrons
523 are placed into the rack inside the boxes and 500 mL of water is added to the box.

524 **Plant growth** *Arabidopsis thaliana* seeds were stratified for 2 d at 4 °C in Eppendorf tubes
525 with distilled water. Seeds were suspended in 0.1 % agar and 5 to 10 were sown using
526 a transfer pipette in the rhizotron. A transparent acrylic sheet was mounted on top of
527 the box and sealed with tape to ensure high humidity conditions that enable *Arabidopsis*
528 germination. Three days after sowing, the cover was unsealed to decrease humidity and
529 allow the seedlings to acclimate to a dryer environment. From 3 days after sowing (DAS)
530 to the time the first true leaves emerged, it was critical to ensure that the top part of the
531 rhizotron remained humid for proper germination of the plants. Between three and five DAS
532 the rhizotrons were thinned leaving only the number plants required for that experiment,
533 typically one, except for experiments examining root-root interactions. Unless otherwise

534 stated, all the experiments presented here, treatments were started 10 DAS. Plants were
535 grown under long day conditions (16 h light / 8 h dark) using 20–22 °C (day/night) and
536 150 μ E m⁻¹ s⁻¹. Two types of growth environments were used for experiments. A walk-in
537 growth chamber with fluorescent lightning and a growth cabinet with white LED lights.
538 Relative water content measurements were done as previously described³⁴

539 **qRT-PCR analysis.**

540 Seeds were surface sterilized as described before² and grown in rhizotrons, 100 cm³ pots, or
541 on two types of 1% agar (Duchefa) media containing either 1x MS nutrients (Caisson) and 1%
542 Sucrose, (termed ms media) or 1/4x MS nutrients only (termed ms25 media). Both media were
543 buffered using 0.5 g/L MES and pH was adjusted to 5.7 with KOH. All plants were grown
544 together in a growth cabinet with LED lights under long day conditions (16h day/8h night).
545 Root and shoot tissue was collected separately from individual plants at the end of the day
546 (1 hour before the lights shut off) and at the end of the night (1 hour before lights came on).
547 Three biological replicates were collected for each condition. RNA was extracted using the
548 Plant RNA MiniPrepTM kit (ZYMO Research) according to manufacturer's instructions
549 with on-column DNase treatment (Qiagen). cDNA was made using the iScript Advanced
550 cDNA Synthesis for RT-qPCR kit (Bio-Rad) from 200 ng of total RNA. qRT-PCR was
551 performed using a Fluidigm BioMarkTM 96.96 Dynamic Array IFC with the EvaGreen®
552 (Bio-Rad) fluorescence probe according to the Fluidigm Advanced Development Protocol
553 number 37. For the analysis, all the reactions with no amplification ($C_t = 999$) were set to
554 the maximal C_t for that assay type. The two technical replicates were then averaged and
555 dC_t values calculated using AT3G07480, AT4G37830, At1g13320 and At1g13440 as reference
556 internal controls. PCA plots were generated with Devium Web³⁵ using dC_t values. dCT
557 values were calculated as $dCT = CT_{\text{gene interest}} - \text{mean}(CT_{\text{reference gene}})$. Primers
558 used are listed in file Supplement 8.

559 **Biological components**

560 **Codon optimization of luciferases.** The following luciferases that emit light at different
561 wavelengths were codon optimized for Arabidopsis (Genscript, Piscataway, NJ): LUC2: a
562 yellow improved version (Promega, Madison, WI) of the original *Photinus pyralis* (firefly)
563 LUC.

- 564 • Ppy RE8: a red variant³⁶ of the *P. pyralis* thermostable variant Ppy RE-TS³⁷.
- 565 • CBG99: a green variant (Promega, Madison, WI) from yellow click beetle (*Pyrophorus*
566 *plagiophthalmus*) luciferases.
- 567 • CBR: a red variant (Promega, Madison, WI) from yellow click beetle.

568 **Non-optimized luciferases.** We also used the following non-optimized luciferases:

- 569 • nanoLUC: a blue luciferase isolated from a deep sea shrimp¹⁴.
- 570 • venusLUC2: a venus-LUC2 fusion reported to show higher luminescence output than
571 LUC2¹².
- 572 • A transposon containing the bacterial luciferase-containing LUX operon was inte-
573 grated into the *Pseudomonas fluorescens* CH267²⁰ genome by conjugation with *E.*
574 *coli* SM10 *pir* containing pUT-EM7-LUX³⁸ and used to track root microbe coloniza-
575 tion. For inoculation 9 DAS plants were inoculated with 2 mL of an overnight bacterial
576 culture resuspended in 10 mM MgSO₄ and diluted to 0.01 OD.

577 **Generation of single-reporter transgenic plants.** We generated transcriptional fu-
578 sions of all luciferases to constitutive promoters to examine the activity level and emission
579 spectrum of each isoform. The *attL1-attL2* entry clones containing plant-codon optimized
580 coding sequence of *LUC2*, *PpyRe8*, *CBG99* and *CBR* were synthesized by Genscript. A
581 DNA fragment including the *UBQ10* promoter region and first intron was amplified from
582 Col-0 genomic DNA with primers incorporating the attB1, attB4 combination sites at the 5'

and 3' respectively. The PCR product was then introduced into pDONR™ P4-P1R (Invitrogen) through a classic Gateway BP-reaction. The resulting plasmid, the *attL1-attL2* entry clones with luciferase sequences, an empty *attR2-attL3** entry clone and the destination vector dpGreenmCherry² were used to construct *ProUBQ10:LUC2o*, *ProUBQ10:PpyRE8o*, *ProUBQ10:CBG99o* and *ProUBQ10:CBrO* through Gateway LR reactions. The destination vector *dpGreenmCherry* contains a plasma membrane-localized mCherry coding sequence driven by the 35S promoter and is used as a selectable marker of transformation at the mature seed stage². We used Golden Gate cloning and the destination vectors that we had generated before¹³ for the following fusions: *ProUBQ10:nanoLUC2*, *ProUBQ10:venusLUC*, *ProACT2:PpyRE8o*. Briefly, the different components of each construct were PCR amplified with complementary BsaI or SapI cutting sites, mixed with the destination vector in a single tube, digested with either BsaI or SapI, ligated with T4 DNA ligase, then transformed into *E. coli* Top10 cells and plated on LB antibiotic plates containing X-gal as previously described¹³. Junction sites were confirmed by sequencing. We used pSE7 (Addgene ID #: pGoldenGate-SE7: 47676) as the destination vector of the *ProUBQ10:nanoLUC2*, *ProUBQ10:venusLUC* constructs and pMYC2 (Addgene ID #: pGoldenGate-MCY2: 47679) as the destination vector for *ProACT2:PpyRE8o*. Maps of all the vectors can be found in Supplement 8. *ProUBQ10:LUC2o* was transformed into Col-0, Bay and Sha accessions, the *tir1-1*³⁹ mutant and the *miz1*⁴⁰ T-DNA insertion line (SALK_126928).

Brachypodium distachyon The *Arabidopsis* plant-codon optimized Luciferase gene, *LUC2o*, was inserted into the monocot vector pANIC10 via Gateway cloning²⁹. *Brachypodium distachyon* plants were transformed using the method of Vogel and Hill⁴¹.

Tomato The transcriptional fusion *ProeDR5:LUC2* was generated by cloning the *ProeDR5:LUC2* DNA fragment into the pBIB expression vector via restriction sites SalI and Acc65I. The eDR5 promoter is an enhanced version of DR5 containing 13 repeats of the 11-nucleotide core DR5 element⁴² and the pBIB expression vector contains an NPTII resistance gene under the control of the NOS promoter for use as a selectable marker during

610 transformation. All tomato transformations were performed by the Ralph M. Parsons
611 Foundation Plant Transformation Facility (University of California, Davis).

612 **Generation of dual-reporter plants.** To generate dual-reporter plants expressing lu-
613 ciferase isoforms that emit light with divergent emission spectra we used *ProACT2:PpyRE8o*
614 as the root structural marker and ZAT12:LUC¹⁹ and DR5:LUC+¹⁸ lines that were trans-
615 formed with the *ProACT2:PpyRE8o* construct. All constructs were transformed using a
616 modified floral dip method as described in².

617 To make the dual color tomato plants, the *Pro35S:PpyRE8o* transcriptional fusion was
618 generated by putting the plant-codon optimized coding sequence described above into the
619 pMDC32 expression vector through a Gateway LR reaction. The pMDC32 vector con-
620 tains a hygromycin resistance gene under the control of the 35S promoter for use as a se-
621 lectable marker during transformation. This construct was transformed into the transgenic
622 *ProeDR5:LUC2* tomato line.

623 **In vivo emission spectra of plants constitutively expressing luciferase isoforms.**
624 To generate *in vivo* emission spectra of all constitutively expressed luciferases, seeds were
625 sterilized and sown on MS plates as described before². After 8 days, seedlings were treated
626 with a 100 µM luciferin solution, incubated at room temperature for 3 hours and imaged
627 using an IVIS Spectrum imaging system (Perkin Elmer, Waltham , MA) using 20 nm band-
628 pass emission filters at the following wavelengths (in nm: 490-510, 510-530, 530-550, 550-570,
629 570-590, 590-610, 610-630, 630-650, 650-670, 670-690, 690-710). Raw images were analyzed
630 using Fiji and *in vivo* emission spectra were constructed. The full emission spectra of LUX
631 and nanoLUC could not be constructed since the maximum of these two luciferases is below
632 the lower band pass filter that were available.

633 **Imaging system** We designed a custom imaging system (GLO1, Growth and Lumines-
634 cence Observatory 1) optimized for imaging dual-reporter luciferase expression in our custom
635 rhizotrons. The design was a joint effort with Bioimaging Solutions (San Diego, CA) who

636 also built the system and wrote the acquisition software that drives all the mechanical parts
637 of the system. The system is composed by two 2048 x 2048 PIXIS-XB cameras (Princeton
638 Instruments, Trenton, NJ) mounted on top of each other to capture two fields of view en-
639 compassing approximately two 15 x 15 cm areas corresponding to the top or bottom of the
640 rhizotron. The cameras are fitted with a Carl-Zeiss macro lens. A filter wheel with space
641 for four, 76.2 mm filters is positioned in front of the cameras and controlled by a stepper
642 motor allowing for automated changing of the filter wheel position. We used two -542/50
643 and 450/70- custom cut Brightline(R) band-pass filters (Semrock, Rochester, NY). In sin-
644 gle color imaging mode, the filter wheel is operated without filters. Positioned in front of
645 the filter wheel is a removable rhizotron holder mounted on a stepper motor. This stepper
646 motor is also controlled by the GLO-1 software allowing automatic acquisition of images
647 from both sides of the rhizotron sequentially. The whole imaging system is enclosed in a
648 light-tight black box with a door that allows loading and un-loading of rhizotrons.

649 **Plant Imaging** Around 50 mL of 300 μ M D-luciferin (Biosynth, Itasca, IL) was added to
650 soil at the top of the rhizotron. In general 5 min exposures were taken per rhizotron, per
651 side, per channel. For daily imaging experiments, plants were imaged at dawn (+/- 1 hr)
652 to reduce possible effects on diurnal rhythms of keeping plants in the dark during imaging.
653 Shoot images were taken using a Nikon D3100 camera.

654 **Image Preparation** Four individual images are collected: top front, bottom front, top
655 back and bottom back. Using an automated [ImageJ macro](#), a composite image is generated
656 as follows: 1)To correct for differences in background values between the two cameras the
657 mean background value of each image is subtracted from 200; 2) images are rotated and
658 translated to control for small misalignments between the two cameras; 3) the top and
659 bottom images of each side are merged; 4) the back image is flipped horizontally; 5) the
660 front and back images are combined using the maximum values. When dual color images are
661 acquired this operation is repeated for each channel. The final images produced are 16-bit
662 depth and 4096 x 2048 pixels. The scale of the images is 138.6 pixels per cm. Considering

663 that an Arabidopsis roots is 100 μm this results in 1.39 pixels across an Arabidopsis root.

664 **GLO-RIA imageJ plug-in** GLO-RIA uses a combination of existing tools to extract
665 relevant root architecture features. Directionality is acquired using the [directionality plugin](#)
666 from ImageJ. After the number of direction bins (we usually use bins of 2 °) is defined by the
667 user, a 5x5 sobel operator is used to derive the local gradient orientation. This orientation
668 is then used to build a distribution of directions by assigning the square of the orientation
669 into the appropriate bin. Instead of representing the total counts at each orientation a
670 relative value is calculated by dividing the individual values at each bin by the total sum
671 of the histogram (and multiplying by 100). Similar algorithms have been used to quantify
672 dynamic changes in the plant cytoskeleton⁴³.

673 The Elliptic Fourier Descriptors are aquired using the [Fourier Shape Analysis plugin](#) on
674 convex hull shape of the root system. Elliptic Fourier Descriptors have been used in numer-
675 ous studies to analyse variations in shapes, notably in leaves (e.g⁴⁴) The shape analysis is
676 inspired by RootScape¹⁵. Due to the absence of fixed, recognisable structures in root system
677 (that are required for the position of true landmarks), pseudo-landmarks are automatically
678 extracted from the root systems. Shortly, the image is divided vertically at equidistant posi-
679 tions (with the number defined by the user) and for each of the image stripes, the minimum
680 and maximum x coordinates are computed. The shape analysis is therefore able to discrim-
681 inate root system with different vertical root distributions or global root system orientation
682 (e.g. chemotropism) . The code source for the plugin, manual and sample images can be
683 found in the [github repository](#) of the project.

684 Statistical analysis was performed in R⁴⁶. The tidyR⁴⁷, dplyr⁴⁷, gridExtra⁴⁸, shapes⁴⁹,
685 geomorph⁵⁰, ggplot2⁵¹ and cowplot⁵² packages were used for data preparation, analysis
686 and plotting. Final figure preparation was done in [Inkscape](#).

687 **Data availability** All the scripts and original data used to analyze and produce the
688 images can be accessed in the Github repository of the project: github.com/rr-lab/GLO-
689 Roots. Raw files of all the images used in the paper are availabe in [Dryad](#).

690 Acknowledgements

691 Work in the lab of JRD was funded by the Carnegie Institution for Science Endowment
692 and grants from the National Science Foundation (MCB-115795) and Department of En-
693 ergy, Biological and Environmental Research program (DE-SC0008769). RRA was sup-
694 ported by a Carnegie Postdoc Fellowship and currently by Conacyt Ciencia Básica Joven
695 Investigador grant number (CB-2014-01-238101). GL was supported by the Belgian Fonds
696 de la Recherche Scientifique. JM was funded by the National Science Foundation (IOS-
697 0820854). CH is funded by MGH Toteston & Fund for Medical Discovery Fellowship grant
698 2014A051303 and NIH R37 grant GM48707 and NSF grant MCB-0519898 awarded to Fred-
699 erick Ausubel, and previously by the Gordon and Betty Moore Foundation through Grant
700 GBMF 2550.01 from the Life Sciences Research Foundation. JV was funded by the Office
701 of Biological and Environmental Research, Office of Science, US Department of Energy, in-
702 teragency agreements DE-SC0001526 and DE-AI02-07ER64452. We thank Robert Mittler
703 and Philip Benfey for providing seeds of ZAT12:LUC and DR5:LUC+ respectively. We also
704 thank Neil Robbins and members of the Dinneny lab for critical review of the manuscript
705 and suggestions during the development of the project. We greatly appreciate Tim Doyle at
706 the Stanford Small Animal Imaging Facility for providing's advice in using and help with
707 luciferase-based imaging approaches.

708 Competing interests

709 We do not have any competing interests that we are aware of.

946 **References**

- 947 1.Dinneny, J. R. *et al.* Cell identity mediates the response of *Arabidopsis* roots to abiotic
948 stress. *Science* **320**, 942–945 (2008).
- 949 2.Duan, L. *et al.* Endodermal ABA Signaling Promotes Lateral Root Quiescence during
950 Salt Stress in Arabidopsis Seedlings. *Plant Cell* **25**, 324–341 (2013).
- 951 3.Lynch, J. P. & Wojciechowski, T. Opportunities and challenges in the subsoil: pathways
952 to deeper rooted crops. *J. Exp. Bot.* **66**, 2199–2210 (2015).
- 953 4.Brady, N. C. & Weil, R. R. *Elements of the nature and properties of soils*. (Prentice Hall,
954 2009).
- 955 5.Bao, Y. *et al.* Plant roots use a patterning mechanism to position lateral root branches
956 toward available water. *Proc Natl Acad Sci* **111**, 9319–9324 (2014).
- 957 6.Tabata, R. *et al.* Perception of root-derived peptides by shoot LRR-RKs mediates systemic
958 N-demand signaling. *Science* **346**, 343–346 (2014).
- 959 7.Rosquete, M. R. *et al.* An Auxin Transport Mechanism Restricts Positive Orthogravit-
960 ropsism in Lateral Roots. *Current Biology* **23**, 817–822 (2013).
- 961 8.Uga, Y. *et al.* Control of root system architecture by DEEPER ROOTING 1 increases
962 rice yield under drought conditions. *Nat. Genet.* **45**, 1097–1102 (2013).
- 963 9.Postma, J. A. & Lynch, J. P. The optimal lateral root branching density for maize depends
964 on nitrogen and phosphorus availability. *Plant Physiol.* **166**, 590–602 (2014).
- 965 10.Schneider, C. A., Rasband, W. S. & Eliceiri, K. W. NIH Image to ImageJ: 25 years of
966 image analysis. *Nature methods* **9**, 671–675 (2012).
- 967 11.Meijon, M., Satbhai, S. B., Tsuchimatsu, T. & Busch, W. Genome-wide association study
968 using cellular traits identifies a new regulator of root development in. *Nat. Genet.* **46**, 77–81
969 (2013).
- 970 12.Hara-Miyauchi, C. *et al.* Bioluminescent system for dynamic imaging of cell and animal
971 behavior. *Biochem. Biophys. Res. Commun.* **419**, 188–193 (2012).

- 972 13.Emami, S., Yee, M.-C. & Dinneny, J. R. A robust family of Golden Gate Agrobacterium
973 vectors for plant synthetic biology. *Front. Plant Sc.* **4**, 339 (2013).
- 974 14.Hall, M. P. *et al.* Engineered Luciferase Reporter from a Deep Sea Shrimp Utilizing a
975 Novel Imidazopyrazinone Substrate. *ACS chemical biology* **7**, 1848–1857 (2012).
- 976 15.Ristova, D. *et al.* RootScape: a landmark-based system for rapid screening of root
977 architecture in Arabidopsis. *Plant Physiology* **161**, 1086–1096 (2013).
- 978 16.Lobet, G. *et al.* Root System Markup Language: toward a unified root architecture
979 description language. *Plant Physiol.* **167**, 617–627 (2015).
- 980 17.Pagès, L. *et al.* Calibration and evaluation of ArchiSimple, a simple model of root system
981 architecture. *Ecological Modelling* **290**, 76–84 (2014).
- 982 18.Moreno-Risueno, M. A. *et al.* Oscillating gene expression determines competence for
983 periodic *Arabidopsis* root branching. *Science* **329**, 1306–1311 (2010).
- 984 19.Miller, G. *et al.* The plant NADPH oxidase RBOHD mediates rapid systemic signaling
985 in response to diverse stimuli. *Science Signaling* **2**, ra45 (2009).
- 986 20.Haney, C. H., Samuel, B. S., Bush, J. & Ausubel, F. M. Associations with rhizosphere
987 bacteria can confer an adaptive advantage to plants. *Nature Plants* **1**, 15051 (2015).
- 988 21.Mandoli, D. F., FORD, G. A., WALDRON, L. J., NEMSON, J. A. & Briggs, W. R. Some
989 spectral properties of several soil types: implications for photomorphogenesis*. *Plant Cell*
990 *Environ.* **13**, 287–294 (1990).
- 991 22.Galen, C., Rabenold, J. J. & Liscum, E. Functional ecology of a blue light photoreceptor:
992 effects of phototropin-1 on root growth enhance drought tolerance in *Arabidopsis thaliana*.
993 *New Phytol.* **173**, 91–99 (2007).
- 994 23.Moni, A., Lee, A. Y., Briggs, W. R. & Han, I. S. The blue light receptor Phototropin 1
995 suppresses lateral root growth by controlling cell elongation. *Plant Biology* 34–40 (2014).
- 996 24.Yokawa, K., Kagenishi, T. & Baluška, F. Root photomorphogenesis in laboratory-
997 maintained *Arabidopsis* seedlings. *Trends Plant Sci.* **18**, 117–119 (2013).

- 998 25.Lobell, D. B. *et al.* Greater Sensitivity to Drought Accompanies Maize Yield Increase in
999 the U.S. Midwest. *Science* **344**, 516–519 (2014).
- 1000 26.Ort, D. R. & Long, S. P. Limits on Yields in the Corn Belt. *Science* **344**, 484–485 (2014).
- 1001 27.Pacheco-Villalobos, D. & Hardtke, C. S. Natural genetic variation of root system archi-
1002 tecture from Arabidopsis to Brachypodium: towards adaptive value. *Philosophical Trans-
1003 actions of the Royal Society of London B: Biological Sciences* **367**, 1552–1558 (2012).
- 1004 28.Watt, M., Schneebeli, K., Dong, P. & Wilson, I. W. The shoot and root growth of
1005 Brachypodium and its potential as a model for wheat and other cereal crops. *Functional
1006 Plant Biol.* **36**, 960–969 (2009).
- 1007 29.Mann, D. G. J. *et al.* Gateway-compatible vectors for high-throughput gene functional
1008 analysis in switchgrass (*Panicum virgatum L.*) and other monocot species. *Plant Biotechnol.
1009 J.* **10**, 226–236 (2012).
- 1010 30.Pacheco-Villalobos, D., Sankar, M., Ljung, K. & Hardtke, C. S. Disturbed Local
1011 Auxin Homeostasis Enhances Cellular Anisotropy and Reveals Alternative Wiring of
1012 Auxin-ethylene Crosstalk in *Brachypodium distachyon* Seminal Roots. *PLoS Genet* **9**,
1013 e1003564 (2013).
- 1014 31.Buer, C. S., Wasteneys, G. O. & Masle, J. Ethylene modulates root-wave responses in
1015 Arabidopsis. *Plant Physiology* **132**, 1085–1096 (2003).
- 1016 32.Blossfeld, S., Schreiber, C. M., Liebsch, G., Kuhn, A. J. & Hinsinger, P. Quantitative
1017 imaging of rhizosphere pH and CO₂ dynamics with planar optodes. *Annals of Botany* **112**,
1018 267–276 (2013).
- 1019 33.Shaw, S. L. & Ehrhardt, D. W. Smaller, Faster, Brighter: Advances in Optical Imaging
1020 of Living Plant Cells. *Annu. Rev. Plant Biol.* **64**, 351–375 (2013).
- 1021 34.Barr, H. & Weatherley, P. A re-examination of the relative turgidity technique for esti-
1022 mating water deficit in leaves. *Aust. J. Biol. Sci* **15**, 413–428 (1962).
- 1023 35.Grapov, D. DeviumWeb: Dynamic Multivariate Data Analysis and Visualization Plat-

- 1024 form.
- 1025 36.Branchini, B. R. *et al.* Red-emitting luciferases for bioluminescence reporter and imaging
1026 applications. *Analytical Biochemistry* **396**, 290–297 (2010).
- 1027 37.Branchini, B. R. *et al.* Thermostable red and green light-producing firefly luciferase
1028 mutants for bioluminescent reporter applications. *Analytical Biochemistry* **361**, 253–262
1029 (2007).
- 1030 38.Lane, M. C., Alteri, C. J., Smith, S. N. & Mobley, H. L. T. Expression of flagella is
1031 coincident with uropathogenic Escherichia coli ascension to the upper urinary tract. *Proc.
1032 Natl. Acad. Sci. U.S.A.* **104**, 16669–16674 (2007).
- 1033 39.Ruegger, M. *et al.* The TIR1 protein of Arabidopsis functions in auxin response and is
1034 related to human SKP2 and yeast grr1p. *Genes Dev* **12**, 198–207 (1998).
- 1035 40.Moriwaki, T. *et al.* Hormonal Regulation of Lateral Root Development in Arabidopsis
1036 Modulated by MIZ1 and Requirement of GNOM Activity for MIZ1 Function. *Plant Physiol.*
1037 **157**, 1209–1220 (2011).
- 1038 41.Vogel, J. & Hill, T. High-efficiency Agrobacterium-mediated transformation of Brachy-
1039 podium distachyon inbred line Bd21-3. *Plant Cell Rep* **27**, 471–478 (2008).
- 1040 42.Covington, M. F. & Harmer, S. L. The Circadian Clock Regulates Auxin Signaling and
1041 Responses in Arabidopsis. *Plos Biol* **5**, e222 (2007).
- 1042 43.Lindeboom, J. J. *et al.* A Mechanism for Reorientation of Cortical Microtubule Arrays
1043 Driven by Microtubule Severing. *Science* **342**, 1245533–1–1245533–11 (2013).
- 1044 44.Chitwood, D. H. *et al.* A modern ampelography: a genetic basis for leaf shape and
1045 venation patterning in grape. *Plant Physiology* **164**, 259–272 (2014).
- 1046 45.Iwata, H. & Ukai, Y. SHAPE: a computer program package for quantitative evaluation of
1047 biological shapes based on elliptic Fourier descriptors. *The Journal of Heredity* **93**, 384–385
1048 (2002).

- 1049 46.R Core Team. *R: A language and environment for statistical computing*. (R Foundation
1050 for Statistical Computing, 2014). at <<http://www.R-project.org/>>
- 1051 47.Wickham, H. *Tidyr: Easily tidy data with spread() and gather() functions*. (2014). at
1052 <<http://CRAN.R-project.org/package=tidyr>>
- 1053 48.Auguie, B. *GridExtra: Functions in grid graphics*. (2012). at <<http://CRAN.R-project.org/>>
- 1054 <<http://CRAN.R-project.org/package=gridExtra>>
- 1055 49.Dryden, I. L. *Shapes: Statistical shape analysis*. (2013). at <<http://CRAN.R-project.org/>>
- 1056 <<http://CRAN.R-project.org/package=shapes>>
- 1057 50.Adams, D. & Otarola-Castillo, E. Geomorph: An r package for the collection and analysis
1058 of geometric morphometric shape data. *Methods in Ecology and Evolution* **4**, 393–399 (2013).
- 1059 51.Wickham, H. *Ggplot2: Elegant graphics for data analysis*. (Springer New York, 2009).
1060 at <<http://had.co.nz/ggplot2/book>>
- 1061 52.Wilke, C. O. *cowplot: Streamlined Plot Theme and Plot Annotations for ggplot2*. (2015).
1062 at <<http://cran.r-project.org/web/packages/cowplot/index.html>>

₇₁₀ **Tables**

₇₁₁ **Table 1:** Luciferases used in this study.

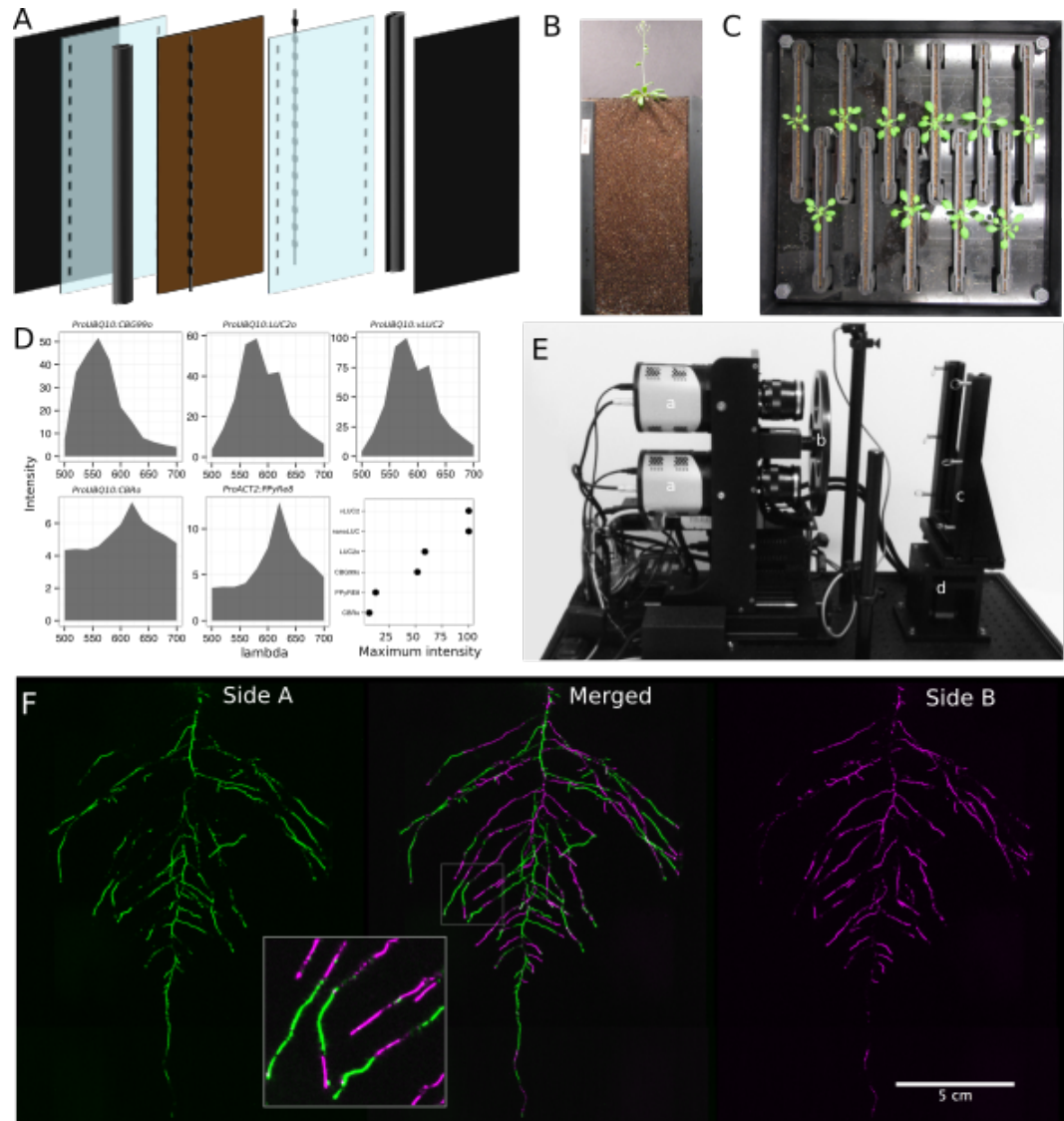
Luciferase	Origin	maximum wavelength	Substrate
Ppy RE8	firefly	618	D-luciferin
CBGRed	click beetle	615	D-luciferin
venus-LUC2	FP + firefly	580	D-luciferin
LUC(+)	firefly	578	D-luciferin
CBG99	click beetle	537	D-luciferin
lux operon	A. fischeri	490	biosynthesis pathway encoded within operon
nanoLUC	Deep sea shrimp	470	furimazine

₇₁₂ **Table 2:** list of root system features extracted using GLO-RIA.

variable	unit
projected area	cm ²
number of visible roots	-
depth	cm
width	cm
convex hull area	cm ²
width	cm
feret	cm
feret angle	°
circularity	-
roundness	-
solidity	-
center of mass	cm
Directionality	°
Euclidean Fourier Descriptors	-

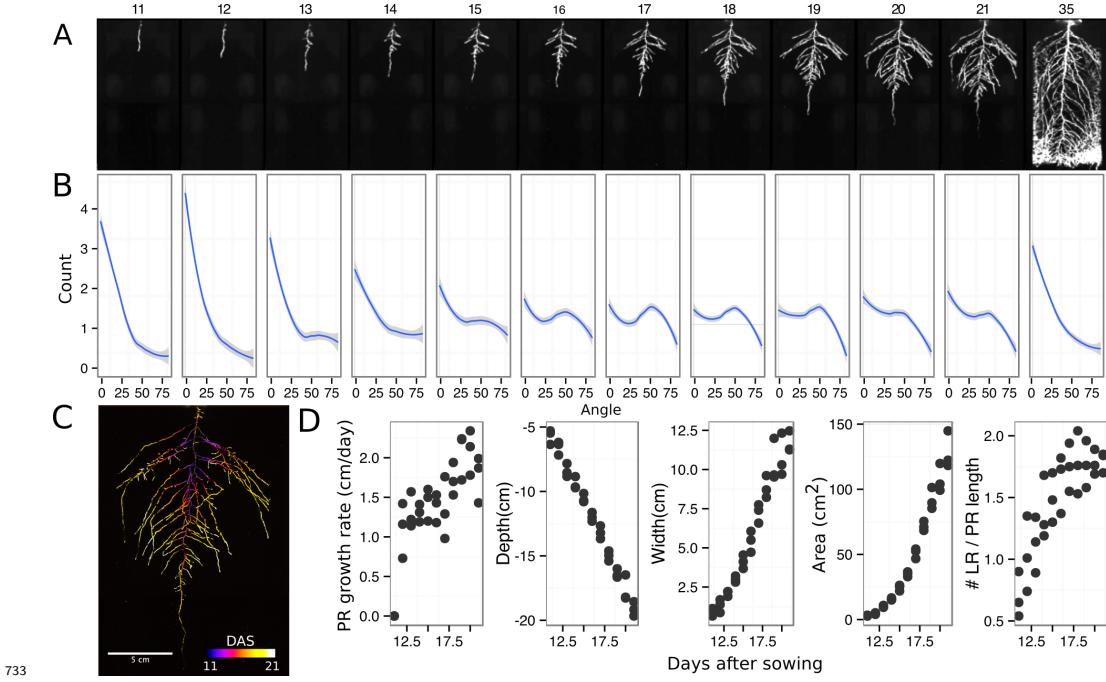
variable	unit
Pseudo landmarks	-

713 **Figures**

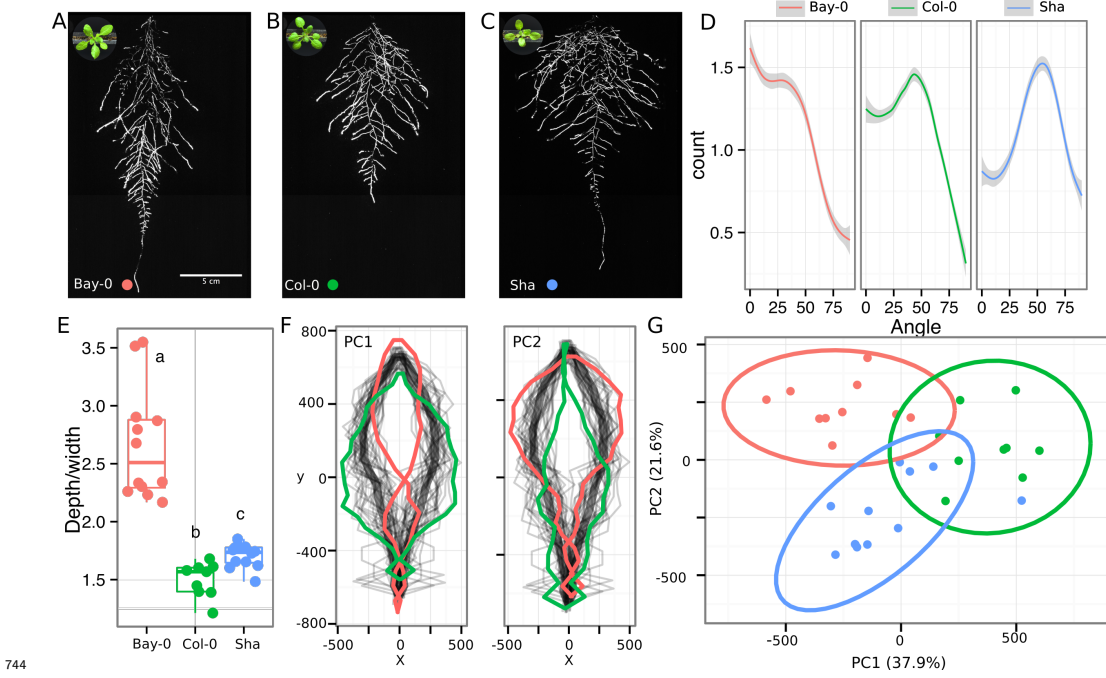


714
715 **Figure 1. GLO-Roots growth and imaging systems** A) 3D representation of the
716 different physical components of the rhizotron: plastic covers, polycarbonate sheets,
717 spacers and rubber U-channels. Blueprints are provided in Supplementary material 1. In brown,
718 soil layer. B) Thirty five day-old plant in rhizotron with black covers removed. C) Top view
719 of holding box with eleven rhizotrons. D)In vivo emission spectra of different luciferases
720 used in this study. Transgenic homozygous lines expressing the indicated transgenes were

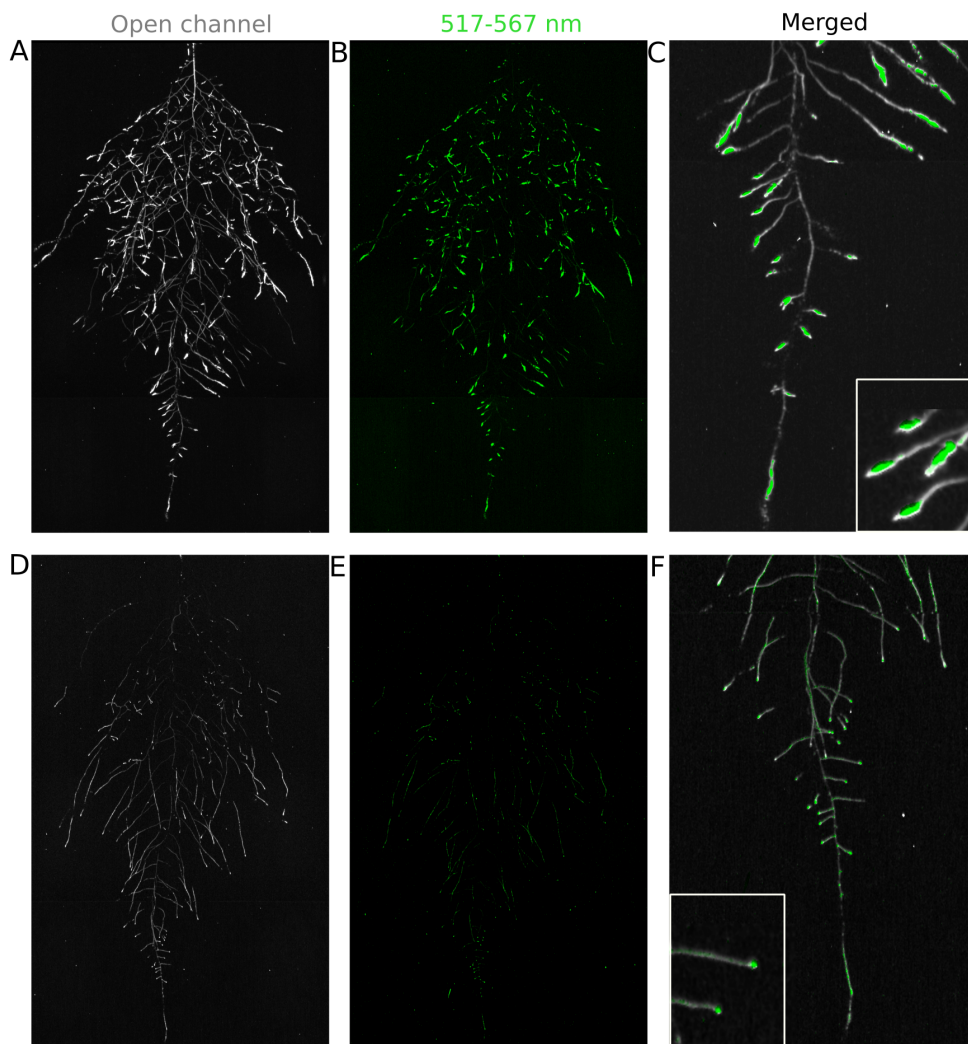
721 grown on agar media for 8 days. Luciferin (300 μ M) was sprayed on the seedlings and
722 plates were kept in the dark and then imaged for 2 s at wavelengths ranging from 500
723 to 700 nm. Five intensity values were taken from different parts of the roots of different
724 seedlings and averaged. Relative maximum intensity values are indicated in the lower right
725 graph. E) GLO 1 imaging system. The system is composed by two back illuminated CCD
726 cameras (a) cooled down to -55 °C. A filter wheel (b) allows for spectral separation of the
727 different luciferases. On the right, a rhizotron holder (c) is used to position the rhizotrons
728 in front of the cameras. A stepper motor (d) rotates the rhizotron 180° to image both
729 sides. F) A 21 DAS plant expressing *ProUBQ10:LUC2o* was imaged on each of two sides
730 of the rhizotron; luminescence signal is colorized in green or magenta to indicate side. In
731 the middle of the panel, a combined image of the two sides is shown. The inset shows a
732 magnified part of the root system. FW: fresh weight, PR: Primary root.



734 **Figure 2. Time-lapse imaging of root systems and quantification using GLO-**
 735 **RIA.** A) Typical daily time-lapse image series from 11 to 35 DAS of a *ProUBQ10:LUC2o*
 736 Col-0 plant. B) Directionality of the root system of plants in panel A calculated using the
 737 directionality plugin implemented in GLO-RIA. C) Color coded projection of root growth
 738 using the images in panel A. D) Primary root growth rate, depth, width, root system area
 739 are automatically calculated from the convex hull, which is semi-automatically determined
 740 with GLO-RIA. Lateral root number and number of lateral roots divided by the primary
 741 root length were quantified manually. A Local Polynomial Regression Fitting with 95%
 742 confidence interval (grey) was used to represent the directionality distribution curve. (0° is
 743 the direction of the gravity vector).



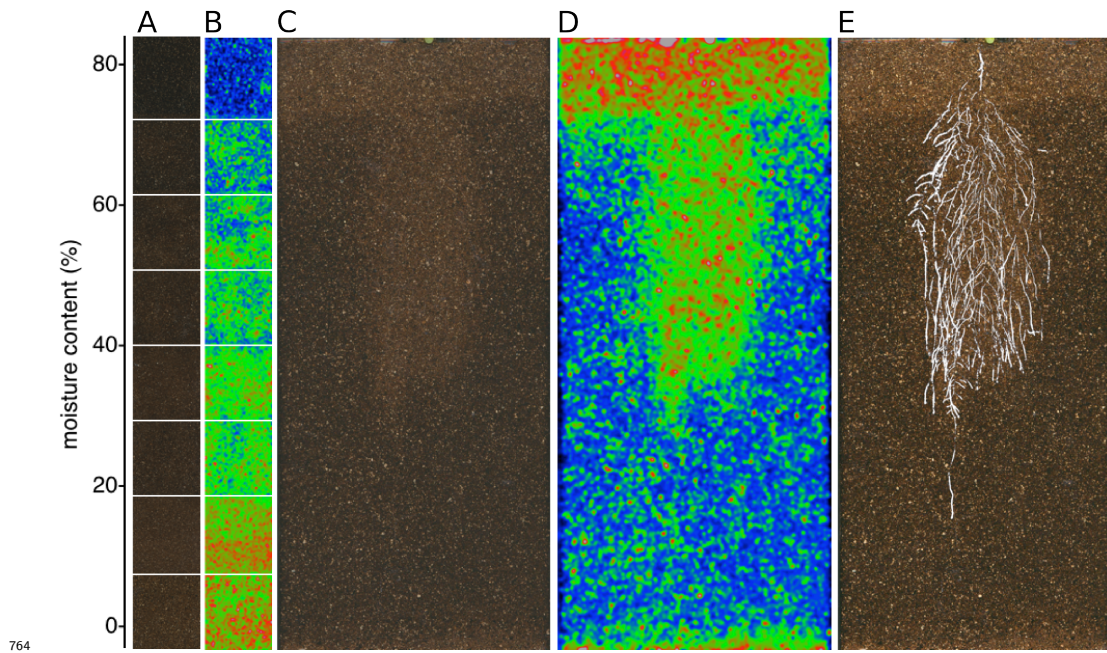
745 **Figure 3. Variation in root architecture between accessions of *Arabidopsis*.** Rep-
 746 resentative root and shoot images of A) Bay-0, B) Col-0 and C) Sha accessions transformed
 747 with `_ProUBQ10:LUC2o` and imaged after 22 DAS. D) Directionality of the root systems,
 748 E) depth/width ratio, F) Pseudo-landmarks describing shape variation in root system archi-
 749 tecture. Eigenvalues derived from the analysis of 9-12 plants per accession is shown. The
 750 first two Principal Components explaining 38% (PC1) and 22% (PC2) of the shape variation
 751 are plotted. PC1 captures homogeneity of root system width along the vertical axis and
 752 PC2 a combination of depth and width in top parts of the root system. Red and green
 753 lines indicate -3SD and +3SD (Standard Deviations), respectively G) PC separation of the
 754 different ecotypes using the PCs described in (F). A Local Polynomial Regression Fitting
 755 with 95% confidence interval (grey) was used to represent the directionality distribution
 756 curve. 0° is the direction of the gravity vector. Wilcoxon test analysis with $p < 0.01$ was
 757 used to test significant differences between the different accession ($n = 9-12$ plants).



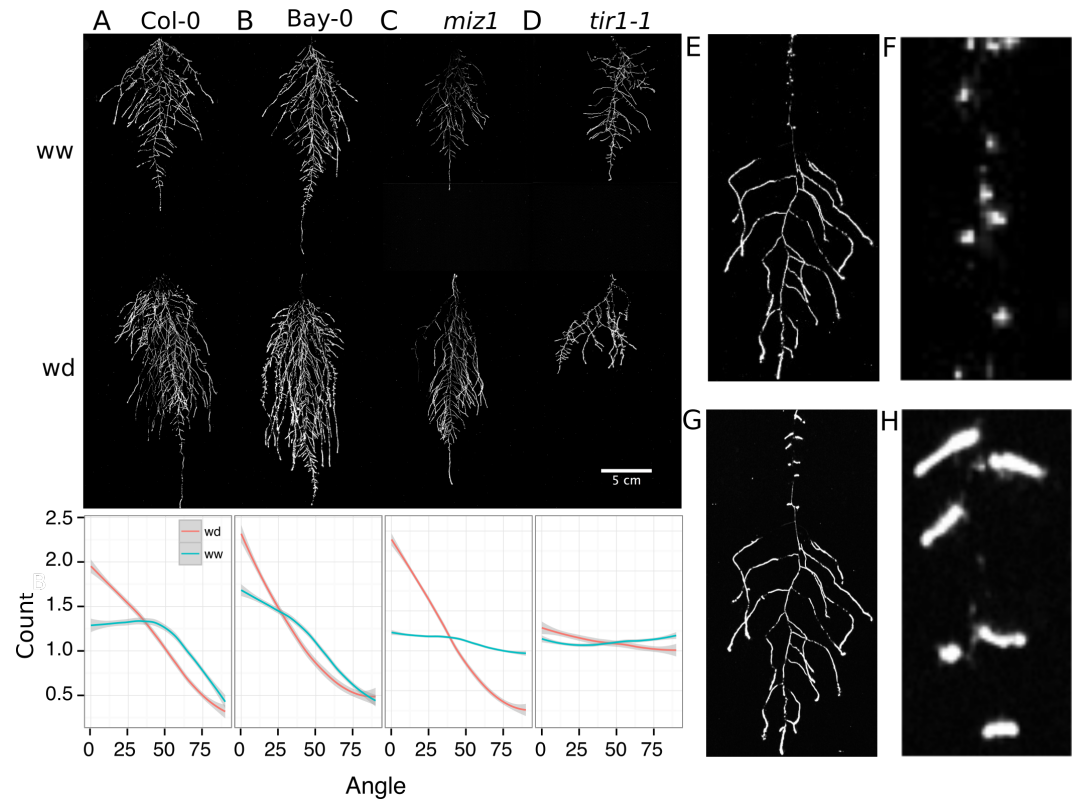
758

759 **Figure 4. Dual-color reporter visualization of structure and gene expression.**

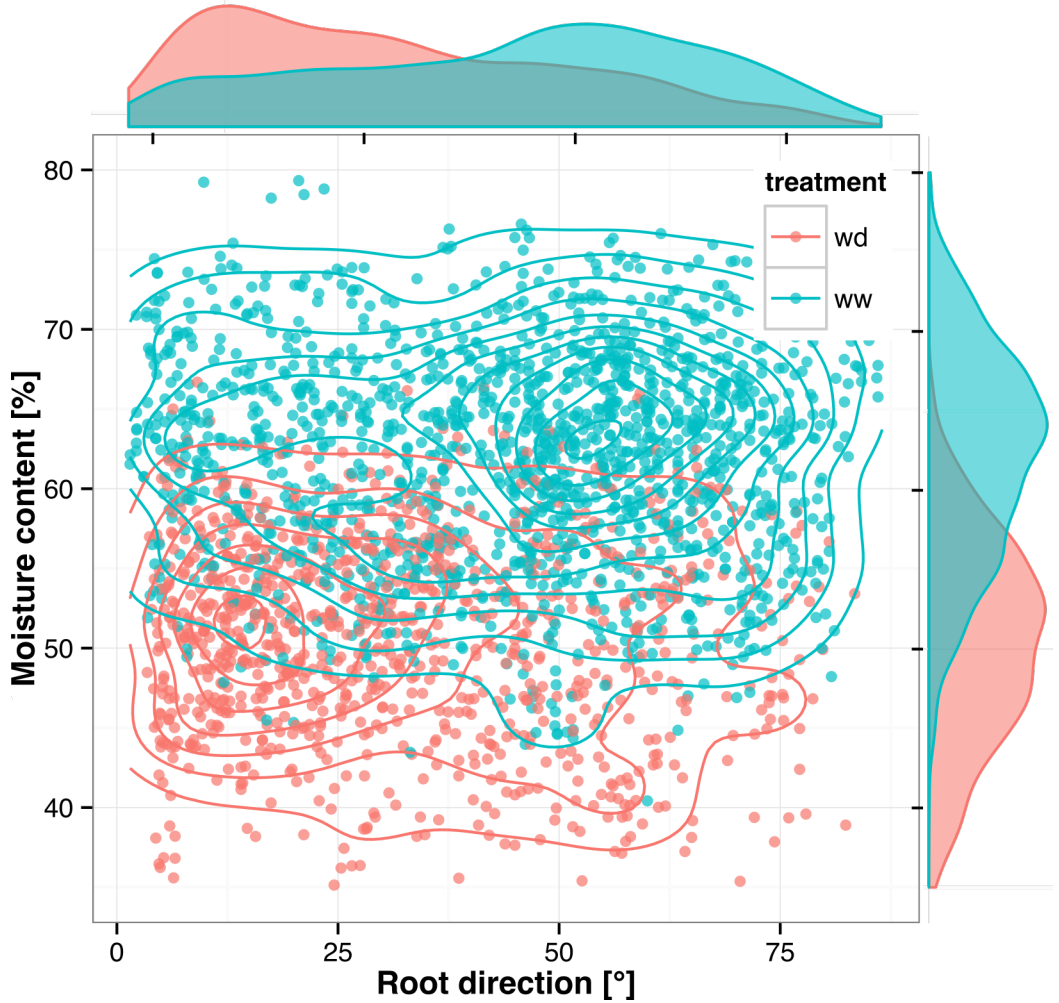
760 Images of whole root systems (A, D) or magnified portion of roots (C, F) at 22 DAS
 761 expressing *ProDR5rev:LUC+* (green, A, B) or *ProZAT12:LUC* signal (green, D, E) with
 762 skeletonized representation of roots generated using the *ProACT2:PpyRE8o* reporter
 763 expression (in grey).



764 **Figure 5. Soil moisture and root architecture mapping in rhizotrons.** A) Com-
 765 posite image showing regions of soil made from rhizotrons prepared with different moisture
 766 levels. B) Differences in grey-scale intensity values were enhanced using a 16-color Look
 767 Up Table (LUT). Brightfield image of soil in rhizotron (C) and converted using 16-color
 768 LUT to enhance visualization of distribution of moisture (D) . E) Root system of a Bay-0
 769 22 DAS and subjected to water deprivation since 13 DAS. Root system visualized using
 770 luminescence and overlaid on brightfield image of soil in (C).
 771

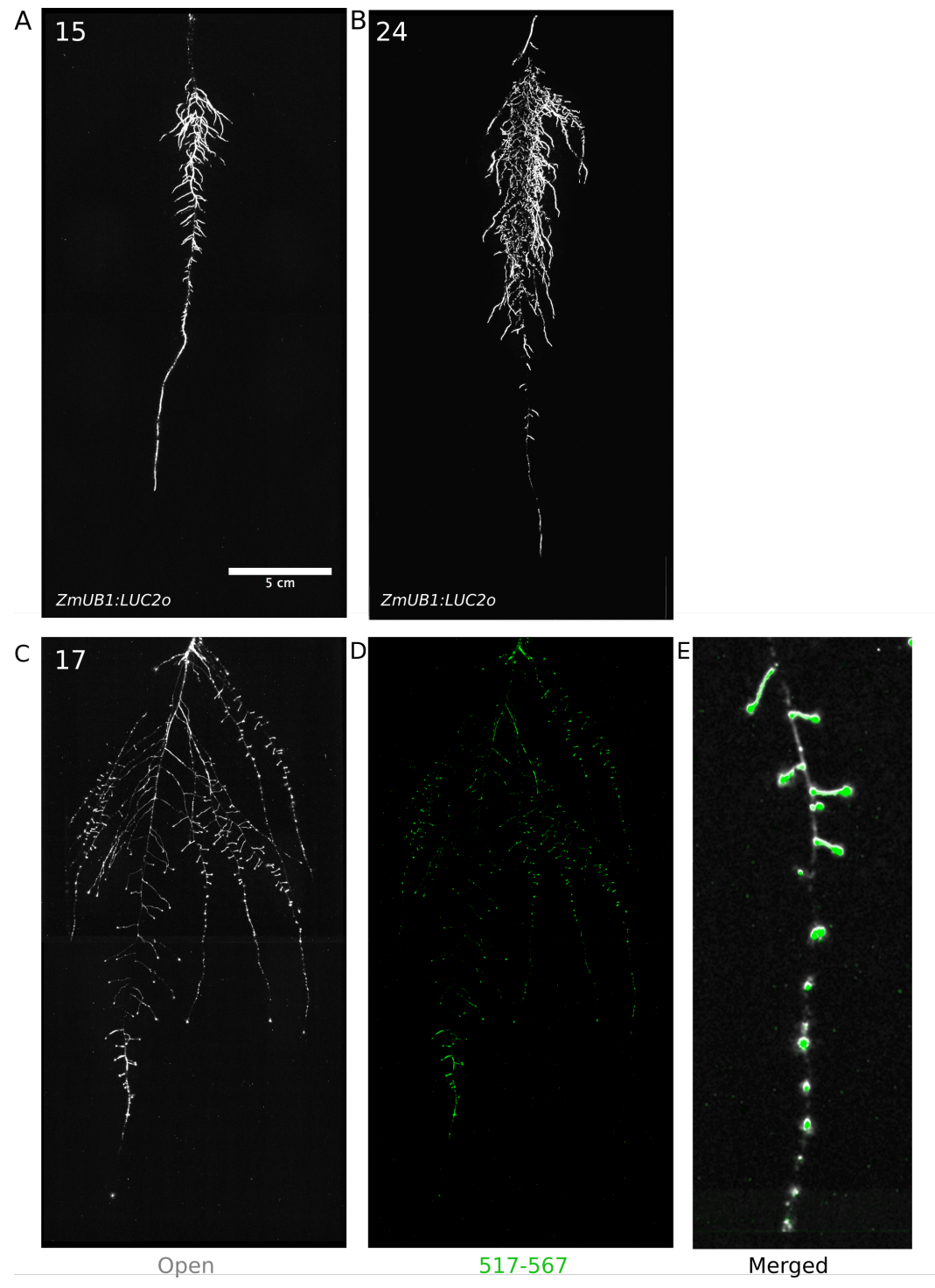


772
 773 **Figure 6. Study of effect of water deficit on root system architecture.** A-D)
 774 Root systems 22 DAS and exposed to water deficit 13 DAS onwards. Sample images of
 775 well watered (left panels) and water deficit (right panels) root systems treated from 13
 776 DAS and directionality (line graphs to left of images) for (A) Col-0 (B) Bay-0 (C) *miz1*
 777 mutant and (D) *tir1-1*. E) Root system of a 22 DAS plant exposed to water deprivation
 778 from 9 DAS onwards with magnified view of lateral root primordia (F). G) The same
 779 root as in (E) 24 hours after rewetting and magnified view of lateral root primordia (H).
 780 Kolmogorov-Smirnov test at $p < 0.001$ was used to compare directionality distributions
 781 between the different treatments and genotypes. A Local Polynomial Regression Fitting
 782 with 95% confidence interval (grey) was used to represent the directionality distribution
 783 curve. 0° is the direction of the gravity vector.



784

785 **Figure 7.** Relationship between local soil moisture content and root growth
 786 direction. Data quantified from the time lapse series shown in [Video 2](#). Density plots
 787 shown at periphery of graph for root direction (x-axis) and soil moisture (y-axis). 0° is
 788 the direction of the gravity vector. Data represents 2535 root tips measured in a series
 789 encompassing 10 time points.



790 **Figure 8:** Roots of *Brachypodium distachyon* transformed with *ProZmUB1:LUC2o* and

792 imaged at 15 (A) and 24 (B) DAS grown in control conditions. C) Open channel of 17
793 DAS tomato plant transformed with *ProeDR5rev:LUC2o* and *Pro35S:PPyRE8o* D) Green
794 channel showing only *ProeDR5rev:LUC2o* E) Amplification of the open and green channel
795 showing increased expression of *ProeDR5rev:LUC2o* reporter in early-stage lateral roots.

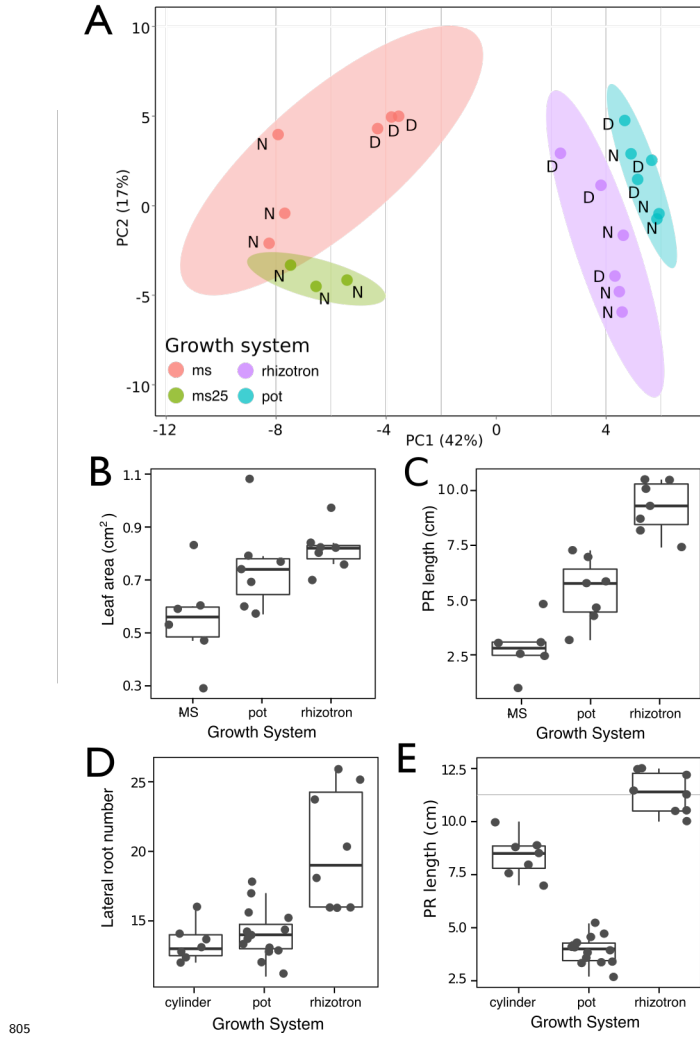
₇₉₆ **Videos**

₇₉₇ **Video 1** Time lapse from 11 to 21 DAS of a Col-0 plant expressing ProUBQ10:LUC2o
₇₉₈ grown in control conditions

₇₉₉ **Video 2** Time lapse from 16 to 24 DAS of Col-0 plants expressing *ProUBQ10:LUC2o*
₈₀₀ growing in water deficient (left) and control (right) conditions. Plants were sown under
₈₀₁ control conditions and water deficit treatment started 11 DAS. Images were taken every
₈₀₂ day.

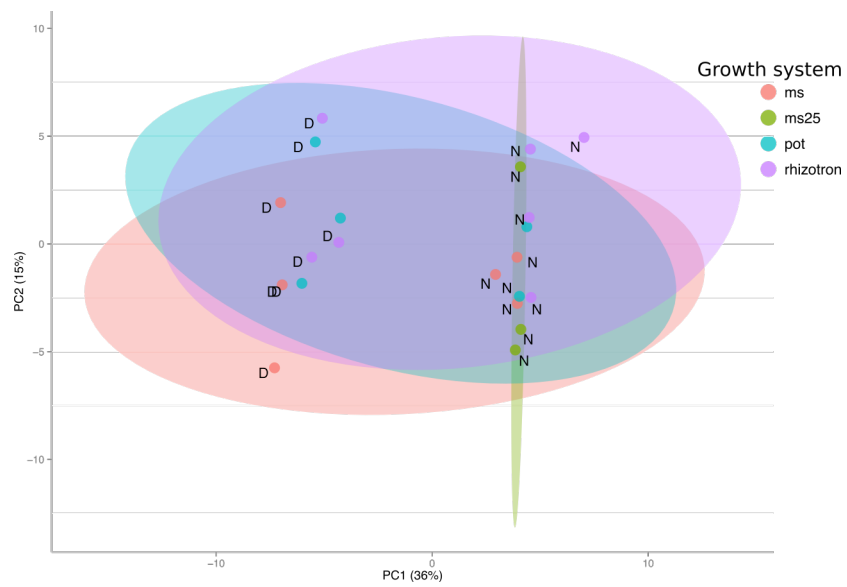
803 **Supplementary Material**

804 **Supplementary figures**



805
806 **Figure 1-figure supplement 1. Effect of different growth systems on plant biol-**
807 **ogy.** A) Principal Components Analysis (PCA) score plot of a set of 76 genes analyzed by
808 qPCR from root samples of plants grown in MS plates, pots, and rhizotrons. After 15 DAS
809 three plants were collected at the end of the day (D) and three were collected at the end of
810 the night (N). (ms = plant grown in full ms and 1% sucrose, ms25 = plants grown in 25%
811 of full ms) B) Lateral root number and G) primary root length of 18 DAS plants grown in

⁸¹² 30 cm tall cylinders, pots and rhizotrons, all with a volume of 100 cm³ (n = 6-12 plants).
⁸¹³ D) Leaf area and E) primary root length of plants of the same age (15 DAS) as the ones
⁸¹⁴ used for the qPCR experiment (n= 6-7). ANOVA analysis with p < 0.01 was used to test
⁸¹⁵ significant differences between the different parameters.



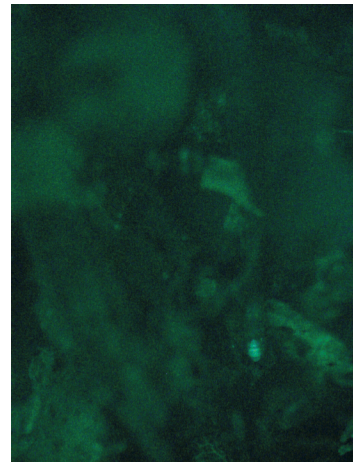
⁸¹⁶ *Figure 1-figure supplement 2. PCA plot of shoots of the same samples analyzed in Figure

⁸¹⁷ 1. See Figure 1 for more details regarding experimental conditions used.



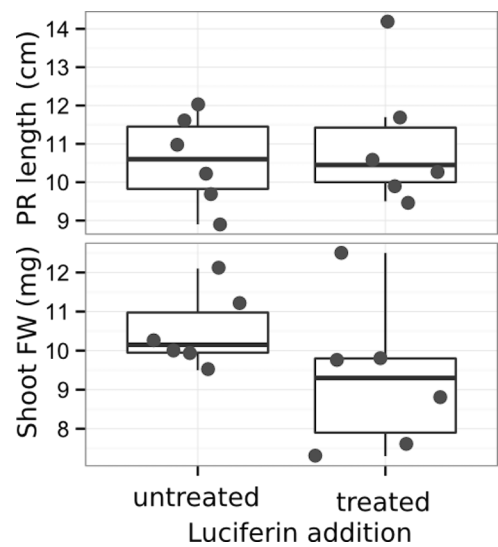
Brightfield

819



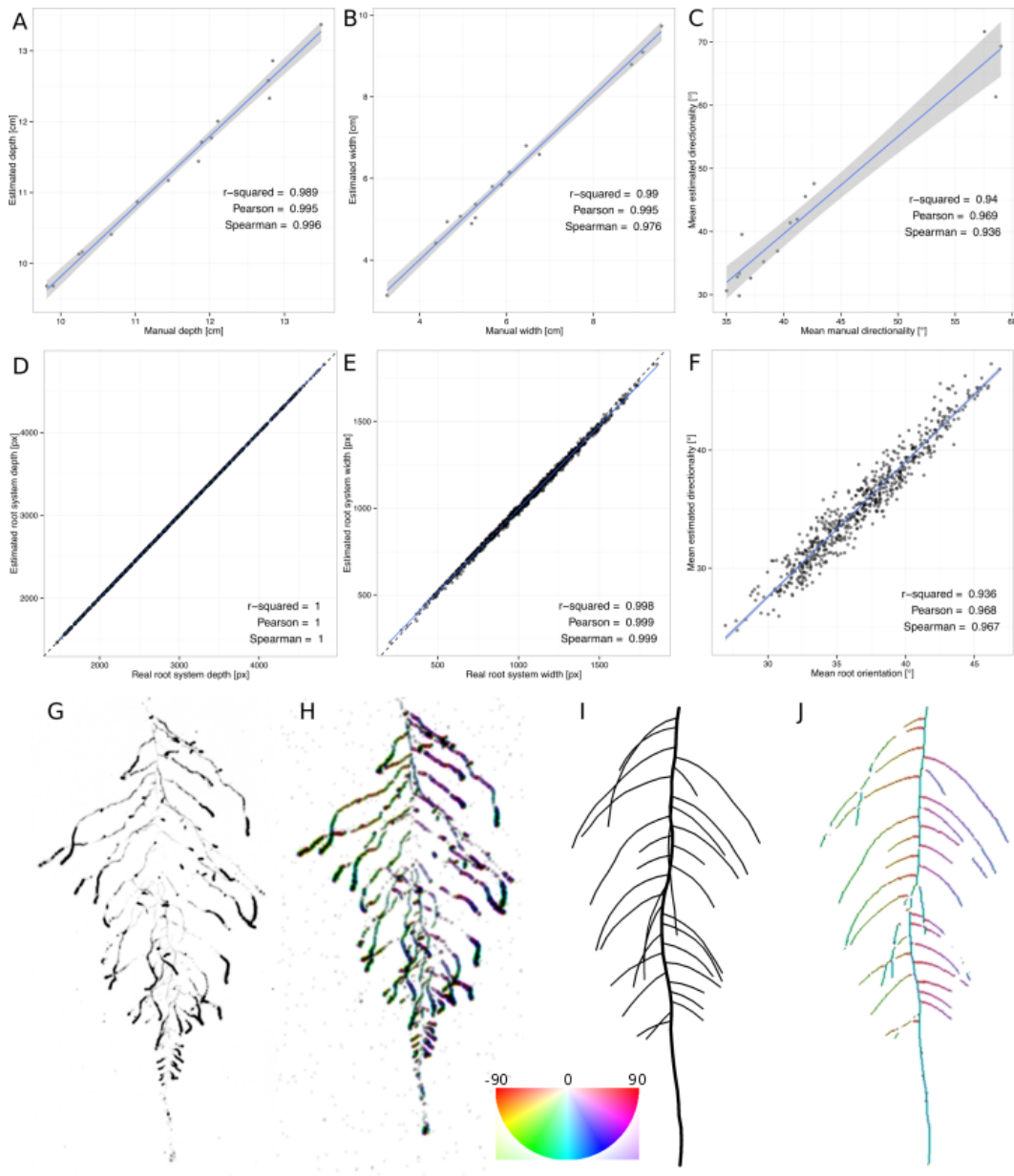
GFP

820 **Figure 1-figure supplement 3** Image of an Arabidopsis root in soil imaged with white
821 light (brightfield) or epifluorescence.



822

823 **Figure 1-figure supplement 4** Effect of luciferin addition on primary root length and
 824 shoot size of 14 DAS seedlings that were either continuously exposed to 300 μM luciferin
 825 from 9 DAS after sowing or not.



826

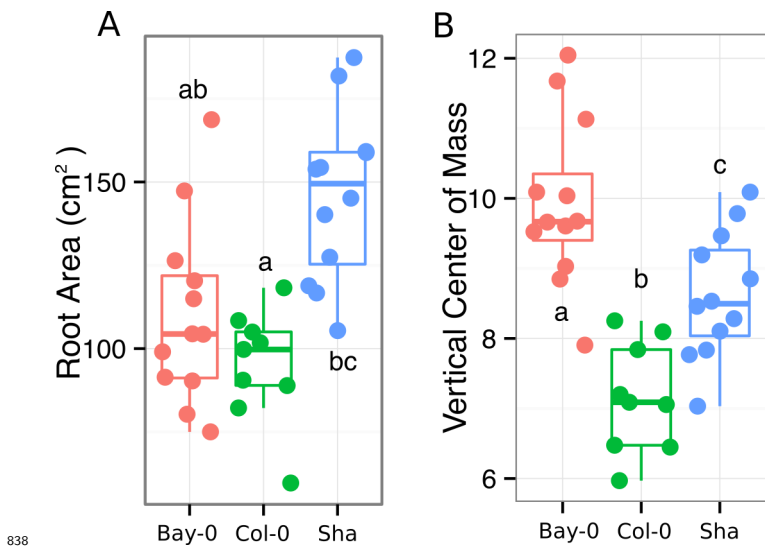
827 **Figure 1-figure supplement 5** GLO-RIA ground truth comparison. Tests of GLO-RIA
 828 were performed using two approaches. We first manually quantified root system depth (A)
 829 width (B) and average lateral root angle (C) in a set of 15 root systems corresponding
 830 to different *Arabidopsis* accessions. We also generated 1240 contrasting root systems
 831 using ArchiSimple and quantified root system depth (D) width (E) and directionality

⁸³² (F) using GLO-RIA. Example of a real (G) and ArchiSimple generated (H) root system

⁸³³ and corresponding GLO-RIA determined directionality color-coded into the image (I, J).

⁸³⁴ Absolute orientation angle values are taken before all calculations.

⁸³⁵ **Figure 1-figure supplement data 1:** Two way ANOVA P-values comparing plants grown
⁸³⁶ in MS media vs. plants grown in soil (pots or rhizotrons) and plants collected at day or night.
⁸³⁷ We used p-value < 0.00065 threshold based on Bonferoni adjustment for multiple testing.



839 **Figure 3-figure supplement 1** A) root area, B) vertical center of mass of Bay-0, Col-0
840 and Sha accessions.

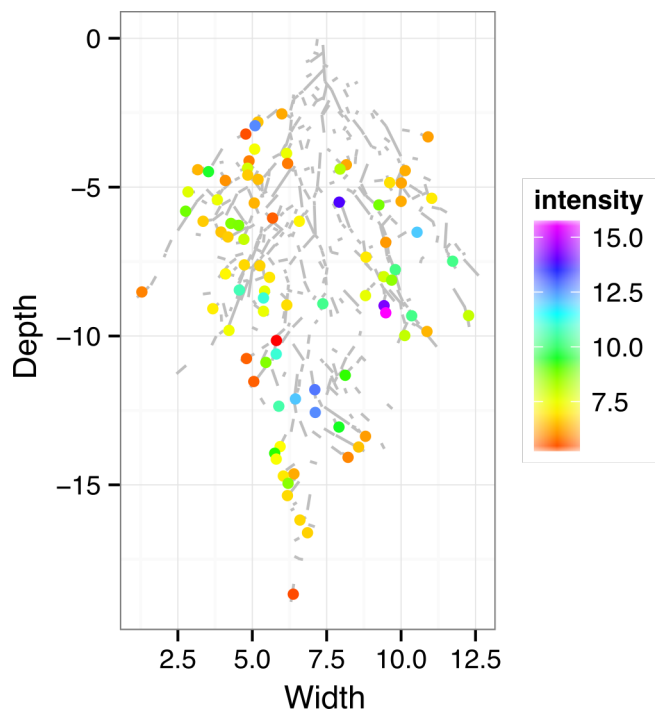
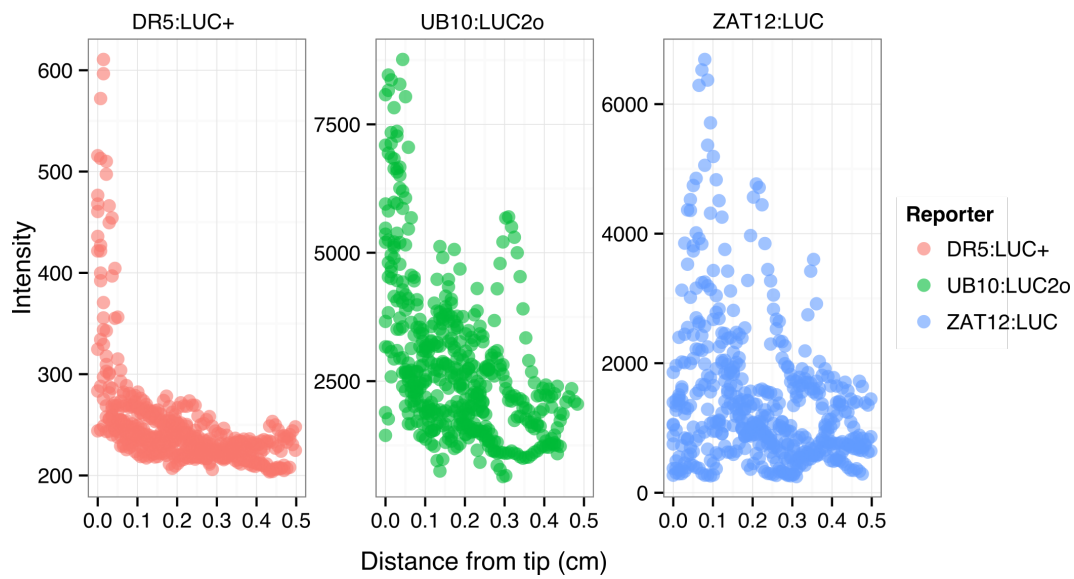


Figure 4-figure supplement 1:

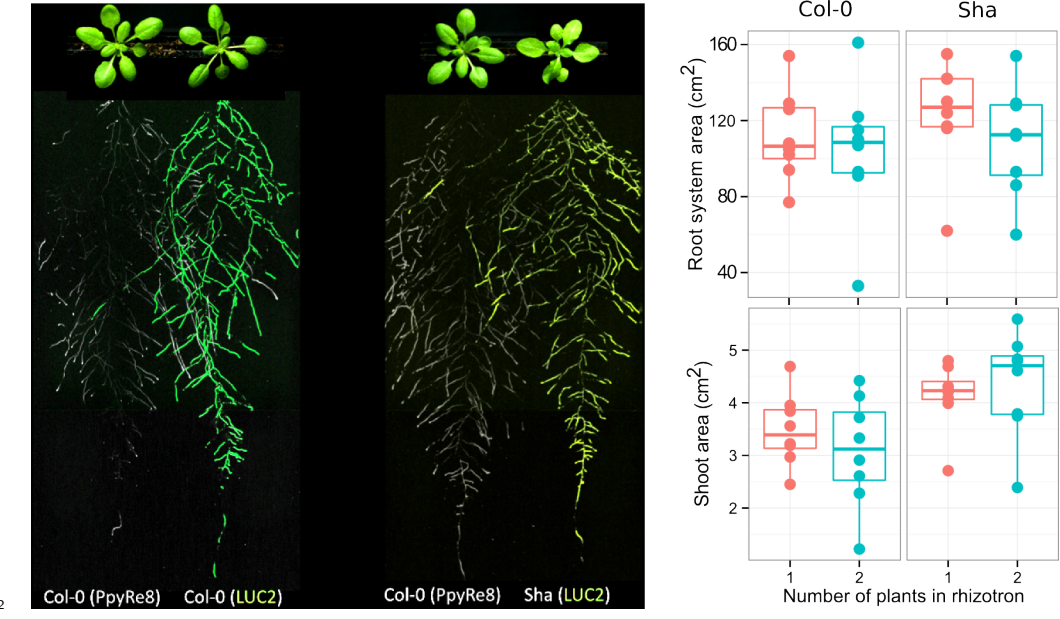
841
 842 ZAT12:LUC intensity and root segments automatically identified values along the root tip.
 843 Data was manually obtained by obtaining the intensity profile of the first 0.5 cm from the
 844 root tip of individual lateral roots. Ten lateral roots for each reporter were measured.
 845



846

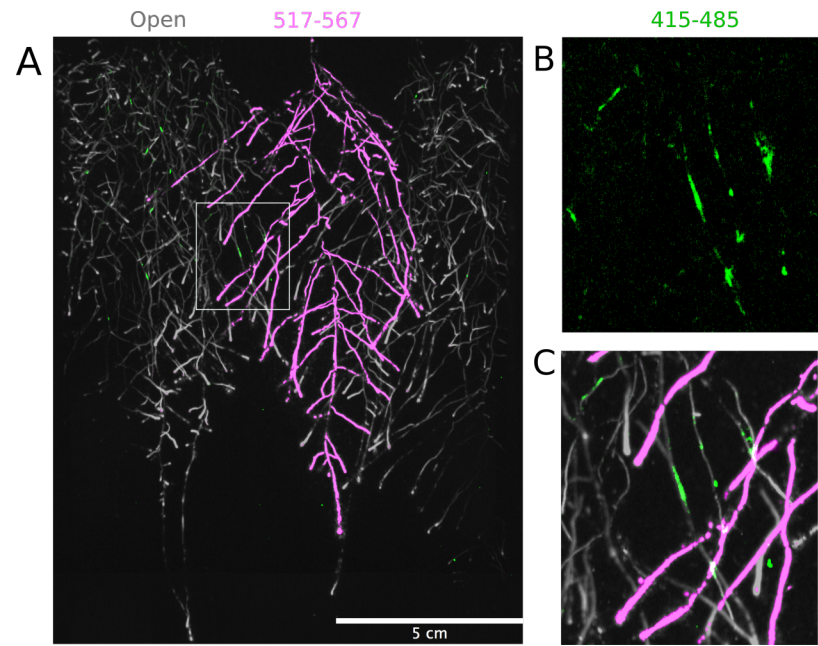
847 **Figure 4-figure supplement 2:** DR5:LUC+, UBQ10:LUC2o and ZAT12:LUC intensity
 848 values along the root tip. Data was manually obtained by obtaining the intensity profile
 849 of the first 0.5 cm from the root tip of individual lateral roots. Ten lateral roots for each
 850 reporter were measured.

851



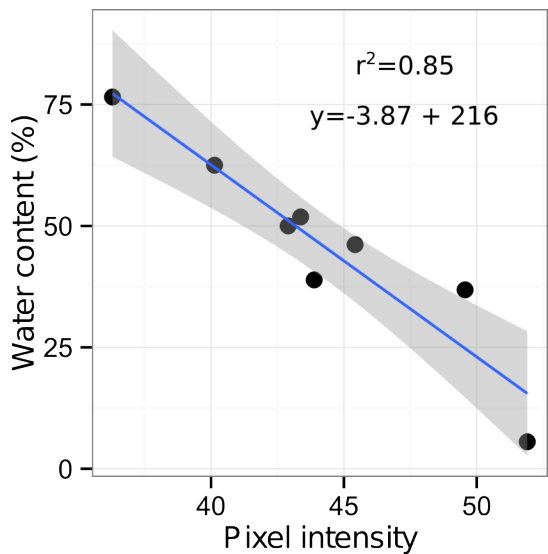
853 **Figure 4-figure supplement 3.** Images of plants at 22 DAS growing in the
 854 same rhizotron and expressing different luciferases. A) Two Col-0 plants expressing
 855 *ProUBQ10:LUC2o* and *ProACT2:PPyRE8o* B) Col-0 plant expressing *ProACT2:PPyRE8o*
 856 and Sha plant expressing *ProUBQ10:LUC2o*.

857



858
 859 **Figure 4-figure supplement 4. Three-reporter-based analysis of root-root-**
 860 **microbe interactions.** A) Image showing a 22 DAS *ProUBQ10:LUC2o* plant (magenta)
 861 grown in the same rhizotron with *ProACT2:PpyRE8o* plants (grey). Plants were inoculated
 862 with *Pseudomonas fluorescens* CH267 (green). Magnified portion of root systems colonized
 863 by *Pseudomonas fluorescens* showing *P. fluorescences* (B) only or all three reporters
 864 together (C).

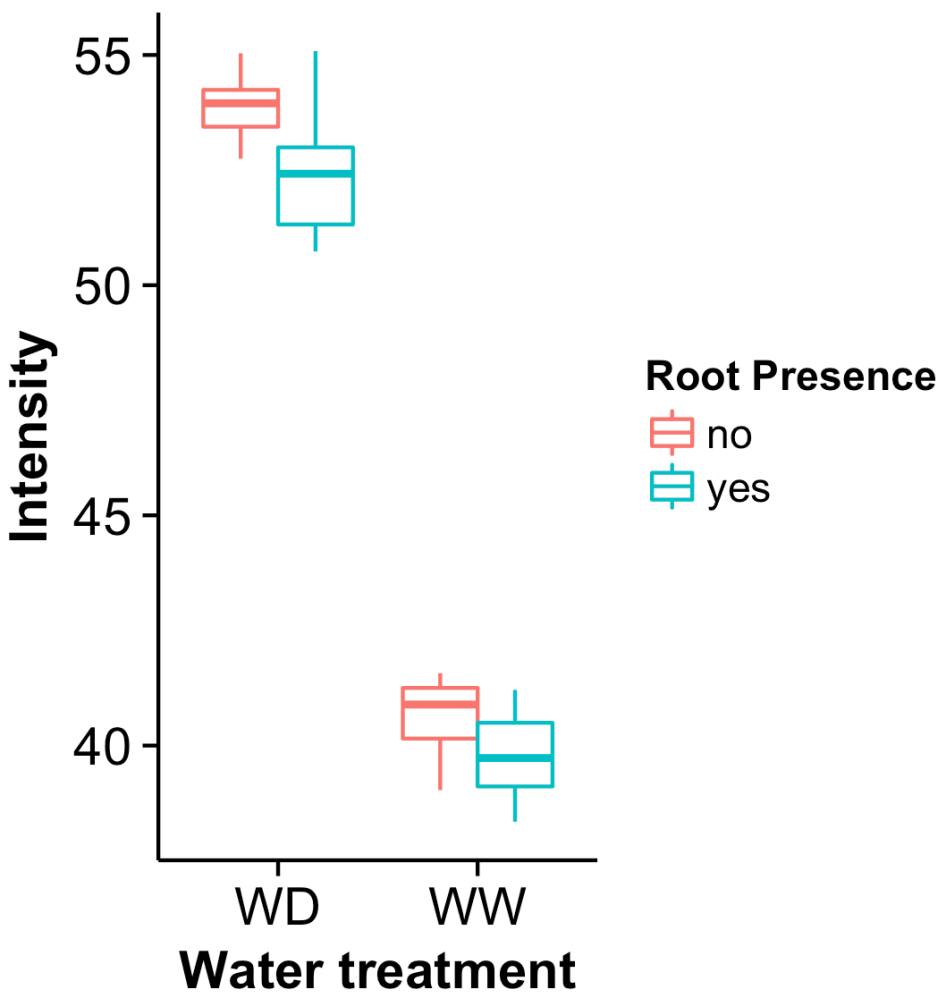
865



866

867 **Figure 5-figure supplement 1:** Moisture calibration curve. Rhizotrons with different
868 levels of moisture were prepared and scanned to obtain readings of pixel intensity. Soil from
869 rhizotrons was then weighed, dried down in an oven at 70 °C for 48 hours and percent water
870 content quantified.

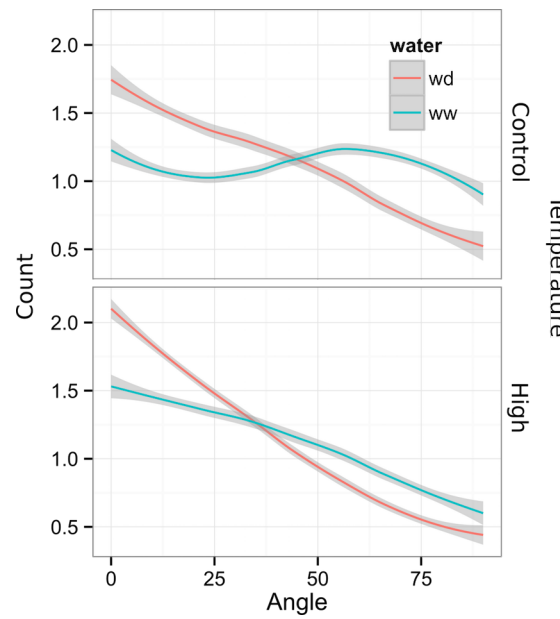
871



872

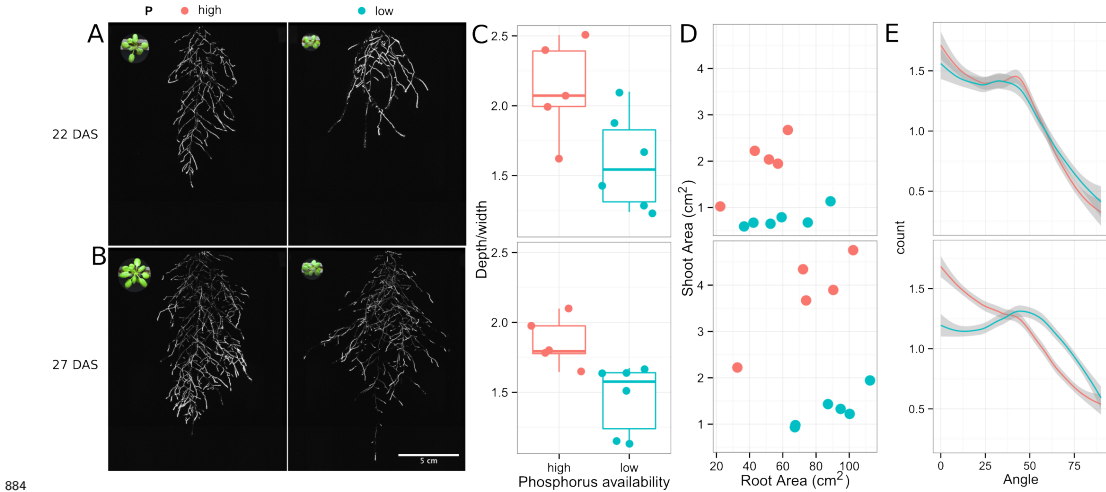
873 **Figure 5-figure supplement 2.** Comparison of soil intensity values between
 874 areas of the rhizotron with or without the presence of roots, determined based
 875 on luminescence data. Mean intensity values from 100 x 100 pixel squares samples of
 876 both areas were obtained from 10 different rhizotrons. Wilcoxon test analysis with $p < 0.01$
 877 was used to test significant differences between areas with our without root presence.

878



879 **Figure 6-figure supplement 1** Directionality analysis of roots of plants transferred to
 880 water deprivation conditions after 9 DAS and kept 22 °C (control temperature) and 29 °C
 881 (high temperature) until 22 DAS. (0° is the direction of the gravity vector).

882

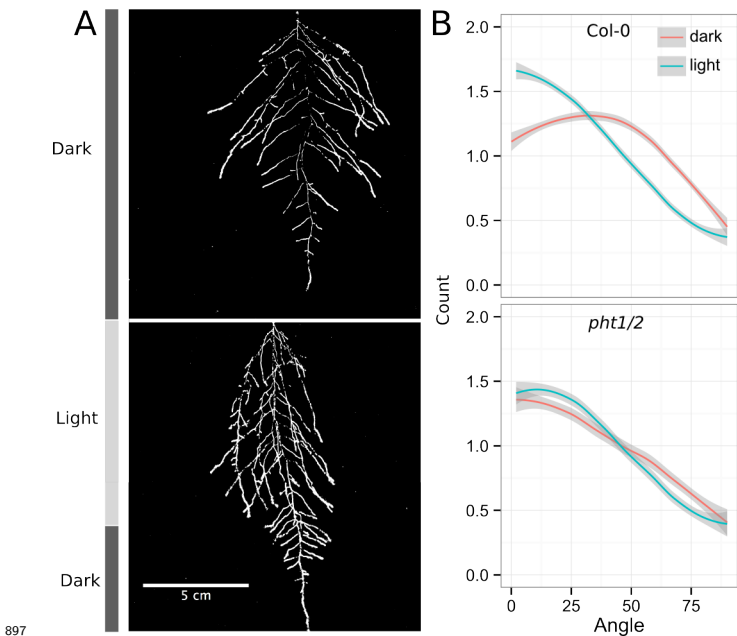


884 **Figure 6-figure supplement 2. Phosphorus deficiency response of root systems**

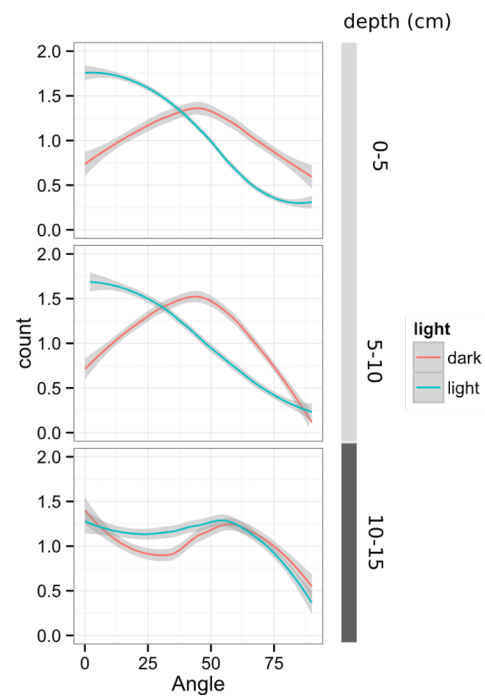
885 Shoot and root systems of *ProUBQ10:LUC2o* Col-0 plants growing in soil supplemented
 886 with 1ml of 100 μ M P-Alumina (left) and 0-P-Alumina (right) 22 (A) or 27 (B) DAS. C)
 887 Root depth/width ratio of 22 (top) and 27 (bottom) DAS plants. D) Scatter-plot showing
 888 relationship between root and shoot system area at 22 (top) and 27 (bottom) DAS. E)
 889 Root directionality distribution in plants 22 (top) and 27 (bottom) DAS. Anova analysis at
 890 p < 0.01 was used to compare depth/width ratios in P treatments. Kolmogorov-Smirnov
 891 test at p < 0.001 was used to compare directionality distributions between the different
 892 treatments. A Local Polynomial Regression Fitting with 95% confidence interval (grey)
 893 was used to represent the directionality distribution curve.(0° is the direction of the gravity
 894 vector).

895

896

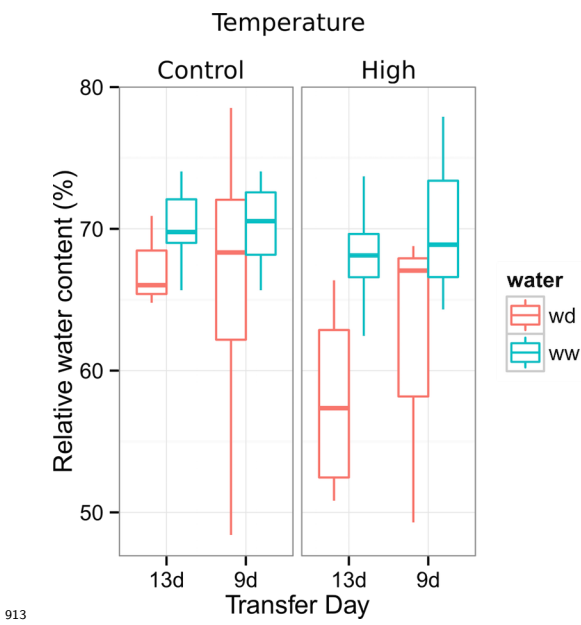


897 **Figure 6-figure supplement 3. Effect of light on root directionality.** A) Col-0
 898 root systems shielded (top) or light exposed (bottom). After 9 DAS the top third of the
 899 rhizotron was exposed to light (indicated on the side with a light grey bar) and plants were
 900 imaged at 20 DAS. B) Directionality analysis of root systems shielded (red) or exposed
 901 (green) to light for Col-0 (top panel) or *pht1/2* double mutant (bottom panel). Between
 902 4 and 6 plants were analyzed per treatment. ANOVA analysis at $p < 0.01$ was used to
 903 compare depth/width ratios in P treatments. Kolmogorov-Smirnov test at $p < 0.001$ was
 904 used to compare directionality distributions between the different treatments. A Local
 905 Polynomial Regression Fitting with 95% confidence interval (grey) was used to represent
 906 the directionality distribution curve. (0° is the direction of the gravity vector).



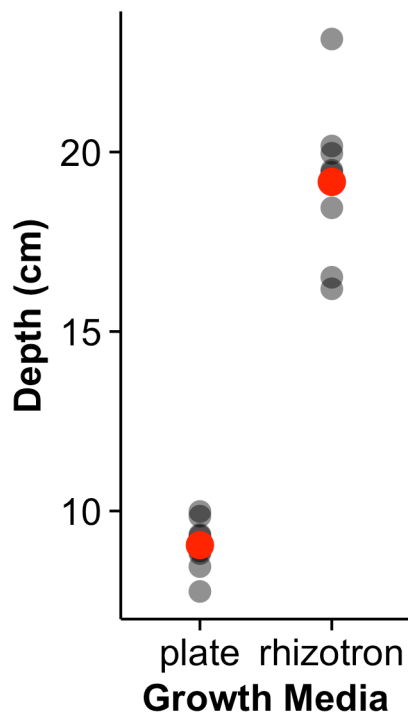
908 **Figure 6-figure supplement 4** Plots showing output of directionality analysis performed
 909 at different depths (0-5, 5-10, 10-15 cm) in rhizotrons exposed to light or kept in the dark.
 910
 911 (0° is the direction of the gravity vector).

912



913 **Figure 6-figure supplement 5.** Leaf relative water content of 23 DAS plants that
 914 were subjected to water deprivation (WD) after 9 or 13 DAS or kept under
 915 well watered (WD) conditions. At 9 DAS half of the plants were kept under control
 916 temperature conditions (22 °C) and the other half transferred to a 29 °C (high) chamber. n
 917 = 6-8 plants.
 918

919



920

921 **Figure 8-figure supplement 1** Depth of the primary root of *Brachypodium* plants grown
922 in rhizotrons or on gel-based media (n=8-11).

923

924 **Supplementary material**

925 **Supplemental Material 1**

926 Blueprints of the holders, clear sheets and spacers needed to built the rhizotrons. Additional
927 details are provided in the materials and methods. Files are provided in Adobe Illustrator
928 .ai and Autocad .dxf formats.

929 **Supplemental Material 2**

930 Primers used in the qPCR experiment.

931 **Supplemental Material 3**

932 Vector maps of all the constructs used in this work.

933 **Source data files**

934 Source data files used for building the following figures are provided: Figure 1-source data 1
935 Figure 1-figure supplement 1-source data 1 Figure 1-figure supplement 2-source data 1 Figure
936 1-figure supplement 3-source data 1 Figure 1-figure supplement 5-source data 1 Figure 2-
937 source data 1 Figure 3-source data 1 Figure 3-source data 2 Figure 3-figure supplement
938 1-source data 1 Figure 4-source data Figure 4-figure supplement 1-source data 1 Figure 4-
939 figure supplement 2-source data 1
940 Figure 5-figure supplement 1-source data 1
941 figure_5_figure_supplement_1.csv
942 Figure 6-source data 1 Figure 6-figure supplement 2-source data 1 Figure 6-figure supplement
943 3-source data 1
944 Figure 6-figure supplement 4-source data 1 Figure 6-figure supplement 5-source data 1 Figure
945 7-source data 1 Figure 8-figure supplement 1-source data 1